3D VISUALIZATION OF MICROGRID

by

Sixuan Duan

A Thesis

Submitted to the Faculty of Purdue University

In Partial Fulfillment of the Requirements for the degree of

Master of Science in Electrical and Computer Engineering

School of Electrical & Computer Engineering

Hammond, Indiana

August 2019

THE PURDUE UNIVERSITY GRADUATE SCHOOL
STATEMENT OF COMMITTEE APPROVAL

Dr. Yao Xu, Chair

Department of Electrical and Computer Engineering

Dr. Xiaoli Yang

Department of Electrical and Computer Engineering

Dr. Bin Chen

Department of Electrical and Computer Engineering

Approved by:

Dr. Vijay Devabhaktuni

Head of the Graduate Program

Dedicated to my parents Wenkui Duan and Honghong Wang

ACKNOWLEDGMENTS

Here, I wish to thank my academic advisor, Dr. Yao Xu for her patient guidance and scientific insight. Since I began my thesis work under her guidance, I have learned much knowledge and many methods for the research. I believe that it will be beneficial for my future career life. Through this thesis project, I not only learn engineering expertise, but also the ethic, dedication and passion for research.

I would also like to thank my other committee members, Dr. Xiaoli Yang and Dr. Bin Chen for their feedbacks. I also wish to thank all my group members in my research for their help and brainstorming.

TABLE OF CONTENTS

LIST OF TABLES

LIST OF FIGURES

LIST OF ABBREVIATIONS

ESS	Energy Storage System
MCC	Motor Control Center
CHP	Combined Heat and Power
PV	Photovoltaic
DG	Distributed Generation
DER	Distributed Energy Resource
UGUI	Unity Graphical User Interface
UI	User Interface

ABSTRACT

Author: Duan, Sixuan. MSECE
Institution: Purdue University
Degree Received: August 2019
Title: 3D Visualization of Microgrid
Committee Chair: Yao Xu

As environment pollution becomes more serious, the use of renewable energy is becoming more and more important. Microgrid is a smart grid that supports intermittent low-carbon energy, designed to provide electricity to the local communities and to connect or disconnect from the main grid. At the same time, considering solar panel and wind turbine as generators. The goal of the microgrid system is to provide each customer with more economical, efficient and reliable power and help customers withstand extreme weather [1]. 3D visualization is to increase the students' interests in the power engineering and vividly shows how the microgrid works.

This thesis first applies the droop control to the existing base MATLAB Simulink model, then designed a 3D visualization of microgrid using 3ds Max and Unity3D software combined with C# language. This is the first time that the 3D virtualization of power system is introduced and realized. 3D models of Solar Panel, Wind turbine, Energy storage system (ESS), Microgrid motor control center (MCC), etc. are built through 3ds Max modeling software and are imported to the Unity3D software. The operation environment of the microgrid system are displayed in three dimensions through Unity3D. Moreover, the interface and virtual system instructions are designed to further fascinate the students learning and increase their interests.

The built 3D visualization of microgrid can vividly show the details and function of each component in the microgrid. In addition, it can demonstrate the operation of Microgrid with the real-time interaction. The first-time application of Unity3D in the microgrid system laid the foundation for the feasibility of virtual technology in the application of engineering education.

CHAPTER 1. INTRODUCTION

1.1 Motivations

With the increasing environmental pollution problems such as global warming, the development of renewable energy has become more and more important and has received widespread attention. At the same time, the development and utilization of renewable energy has made breakthroughs in many scientific researches. Such as combined heat and power (CHP) applications, solar photovoltaic (PV) modules, small wind turbines, thermal and electrical storage. Meanwhile, controllable loads play an important role in the power supply.[2]

Microgrid is a system with one or more distributed energy sources and associated loads. Since the microgrid can be connected or disconnected from the main grid, it is easy to operate in the grid connection state or in the island circuit mode. At the same time, renewable energy resources such as wind and solar energy can be used as power generation sources. Figure 1.1 shows the general structure of microgrid [1-2].

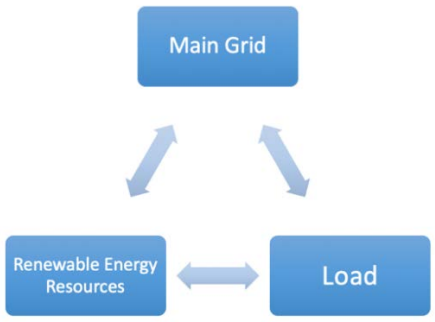

Figure 1.1 General structure of microgrid

With the development of microgrid systems, microgrid control methods have also been widely proposed. At the same time, to enhance the stability of the microgrid system and ensure the normal power supply to the user, a reasonable control method is especially important in the microgrid system.

At the same time, because traditional circuit diagrams often require people with some professional knowledge to understand. And with the rapid development of information

technology, virtual reality has been commercialized and widely applied in research and education. Generally, virtual reality is the computer-generated simulation of a three-dimensional real world which allows participants to experience an artificial environment in an immersive way. The virtual reality system can be widely used in many aspects because it can reproduce the real environment and people can intervene in the interaction [3]. Unity3D and 3ds Max are excellent virtual reality development tools with convenient and realistic modeling capabilities and powerful interactive functions [4]. Due to these reasons, this thesis designed a 3D visualization of microgrid control using 3ds Max and Unity3D software combined with C# language.

1.2 Objectives

Firstly, the goal of this thesis work is to improve the microgrid control system model on the existing MATLAB Simulink base model, and then use the 3ds Max and Unity3D software to achieve 3D visualization. At the same time, the animation effect is added in Unity3D to make the model friendlier.

Based on this model, 3D models of Solar PV, Wind farm, Energy storage system, Microgrid motor control center, etc. are built through 3ds Max modeling software and are imported to the Unity3D software. The operation and control environment of the microgrid system are displayed in three dimensions through Unity3D. At the same time, the Unity3d software simulates the changes in solar and wind energy during the day, increasing the authenticity of the virtual system. Moreover, the interface and virtual system instructions are designed to further fascinate the students learning and increase their interests.

1.3 Thesis Outline

The structure of this thesis paper is organized as follows. Chapter 2 introduces the microgrid control system and one of the control methods (droop control). In Chapter 3, the design methodology of 3D visualization is introducing in detail. Then, Chapter 4 shows the 3D visualization of the microgrid system. Finally, Chapter 5 presents the conclusion of the Unity3D model. In addition, some future works are listed at the end of Chapter 5.

CHAPTER 2. MICROGRID CONTROL SYSTEM

2.1 Microgrid

2.1.1 Background

In global energy use, non-renewable energy (oil, natural gas and coal) accounts for 85% of global energy use. In the United States, 24% of the world's oil is used every year. In China, two-thirds of the energy used each year comes from commercial coal. India imports 50% of its oil and 70% of it comes from highly polluting coal. Over the past 50 years, global energy demand has tripled due to the number of developing countries and technological innovations. It is expected to triple again in the next 30 years [3]. However, non-renewable energy sources such as oil, coal and natural gas are facing depletion of resources [4]. At the same time, with the excessive development and use of traditional fossil energy, serious environmental pollution problems have been caused. It threatens the survival and development of human.

In order to alleviate the contradiction between energy supply and demand and improve people's living environment, countries around the world have accelerated the use and development of renewable energy, mainly based on renewable energy distributed generation (DG). Distributed generation mainly converts renewable energy such as solar energy and wind energy into electrical energy and reduces the demand for fossil energy while making full use of renewable energy. It can effectively alleviate the shortage of power supply caused by insufficient fossil energy. However, the cost of a single unit of distributed generation supply intervening in the main grid is high and the voltage reliability is low. Then the concept of microgrid was put forward [5][6].

2.1.2 Introduction

The microgrid concept [7] was first introduced in the literature [8] and [9] as a solution for the reliable integration of distributed energy resources (DER), including energy storage system (ESS) and controllable loads. Microgrid is a single control unit relative to

the main grid and can meet the user's requirements for power stability. The microgrid has two typical modes of operation, which can be operated in parallel with the external grid or isolated. The switching between the two is smooth and fast.[10]

Figure 2.1[11] shows the typical structure of a microgrid including the interconnection of small, modular generation components (such as solar photovoltaic (PV), wind turbine, etc.), storage devices and controllable loads. This thesis paper will build a microgrid system based on Figure 2.1.

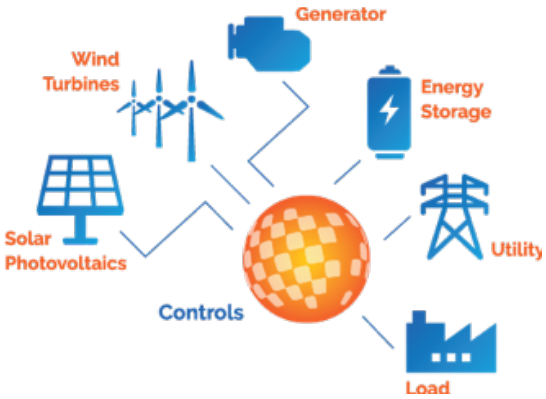

Figure 2.1 Microgrid system

2.2 Microgrid Inverter

2.2.1 Background

At present, the main microgrid power sources are solar energy, wind turbines, and micro gas turbines. Among them, solar energy is converted into electric energy by energy conversion through a photovoltaic cell. However, the photovoltaic battery generates a DC power supply, which requires the help of an inverter to convert the direct current into alternating current to access the AC grid. Wind turbines can eliminate the inverter link and directly access the distribution network. Microturbines mainly use flammable gases such as biogas and natural gas as fuel. However, the high-frequency alternating current that it emits cannot be used directly, and it needs to be rectified and then passed through the inverter to become a commercial frequency alternating current.

Therefore, the microgrid power can be divided into three categories: DC power, DC-AC-DC power, AC power. In the islanded microgrid, the DC power and DC-AC-DC power need to change to the AC power,

The Figure 2.2 shows the structure of islanded microgrid.

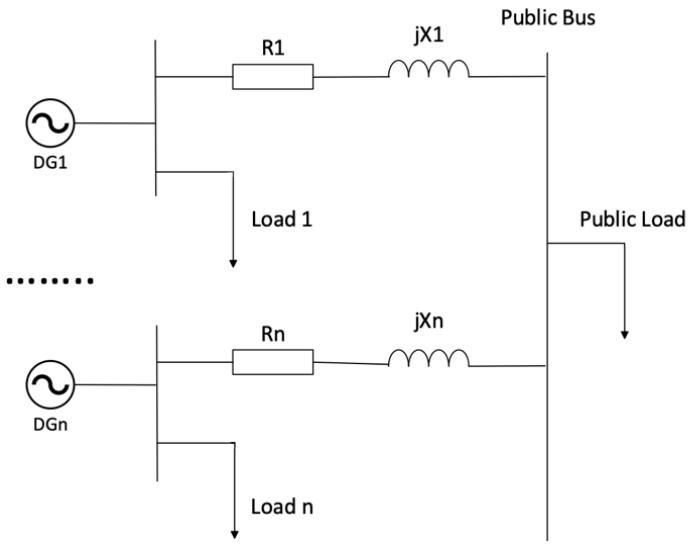

Figure 2.2 The structure of islanded microgrid

2.2.2 Filter

The three-phase inverter uses the PWM to drive the thyristors in the inverter, so that there are harmonics in the output voltage of the inverter, and the harmonics in the voltage can be filtered by using a filter circuit on the output side.

Depending on the device used at the filter exit, common filters are: L-type filter, LC-type filter, LCL-type filter. Among them, the structure of the L filter is the simplest, but requires a larger capacity inverter, which is costly and difficult to control. LCL filter requires two sets of inductors, the parameter values are difficult to select, and the cost is increased. LC filter only needs a set of inductors, which can reduce the cost and control is relatively simple. This thesis paper uses LC filter[12][13]. The Figure 2.3 shows a simple LC filter, the input is a square wave signal that is filtered to a sinusoidal signal[14]. In order to prevent the filter from oscillating, a small resistance resistor is added to the model.

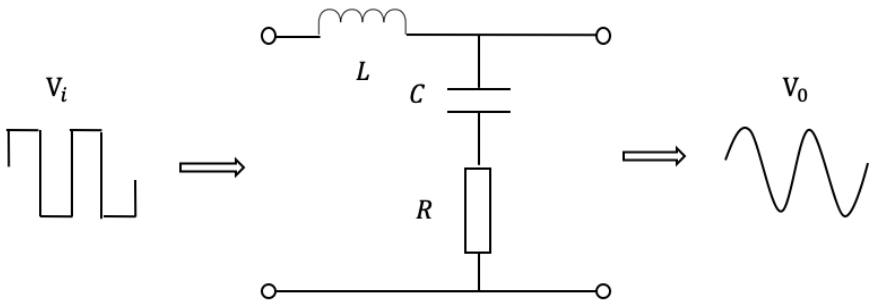

Figure 2.3 LC filter

The transfer function of the LC filter is

$$G(s) = \frac{V_o(s)}{V_i(s)} = \frac{\frac{R}{L}s + \frac{1}{LC}}{s^2 + \frac{R}{L}s + \frac{1}{LC}} \tag{2.1}$$

The cutoff frequency of the LC filter is

$$f_c = \frac{1}{2\pi\sqrt{LC}} \tag{2.2}$$

The cutoff frequency of the LC filter is the most important consideration. In order to filter out the switching harmonics, it should be much lower than the switching frequency. The selection principle of the cutoff frequency of the LC filter should is[14]

$$f_n \ll f_c \ll f_s \tag{2.3}$$

Where, f_n is the fundamental frequency, f_s is the switching frequency.

2.2.3 Inverter Model

Based on Figure 2.2, the topology diagram of the single microgrid power supply three phase inverter is shown in Figure 2.4. Taking solar energy as the power source of the microgrid as an example, the solar energy is equivalent to a DC voltage source (V_{DC}), which is converted into an AC voltage by a three-phase inverter. Since the output voltage of the inverter contains harmonics, a filter circuit is introduced. Through the filter circuit to get the sinusoidal voltage, to provide power for the local load (Z_{abc}).

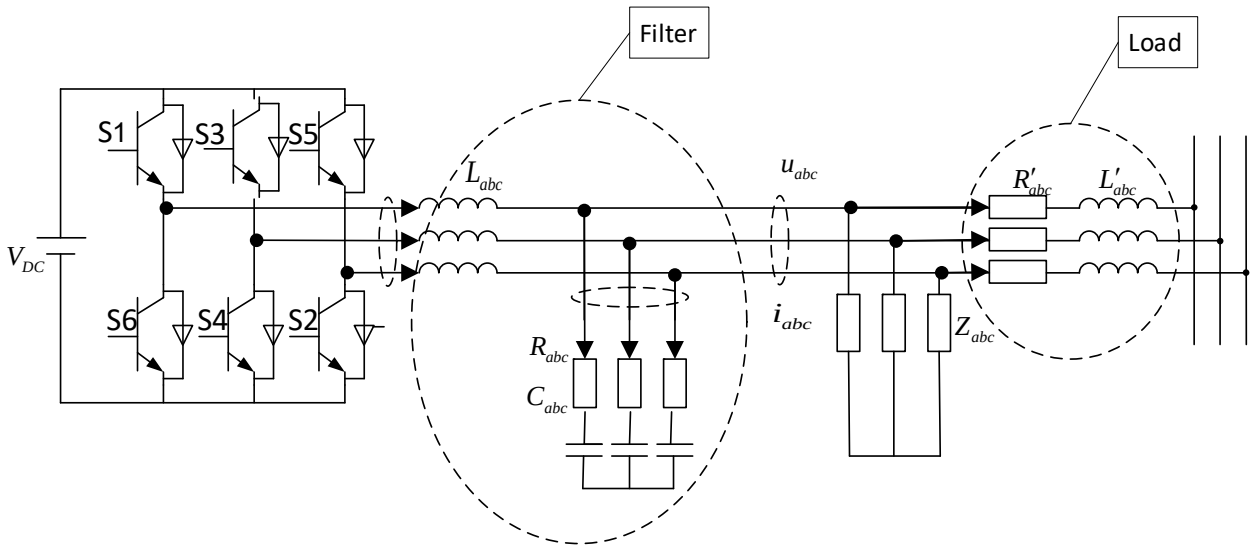

Figure 2.4 Topology diagram of three phase inverter

From the Figure 2.4, the output voltage of a balanced three-phase system in the natural frame (abc frame) equation is

$$\begin{bmatrix} u_a \\ u_b \\ u_c \end{bmatrix} = \begin{bmatrix} V_m cos(\omega t) \\ V_m cos(\omega t - \frac{2\pi}{3}) \\ V_m cos(\omega t + \frac{2\pi}{3}) \end{bmatrix} \tag{2.4}$$

Where, V_m is the peak value of the voltage.

The filter inductor voltage equation is

$$L \frac{di_{Labc}}{dt} = u_{Labc} - u_{abc} \tag{2.5}$$

The filter capacitor current equation is

$$C \frac{du_{abc}}{dt} = i_{Labc} - i_{abc} \tag{2.6}$$

Where u_{Labc} is the voltage vector at the exit of the inverter, i_{Labc} is the current vector at the exit of the inverter, u_{abc} is the filtered output voltage vector, i_{abc} is the filtered output current vector, $L = L_a = L_b = L_c$ is the single phase inductance of the filter, $C = C_a = C_b = C_c$ is the single phase capacitor of the filter.

Combined with equation (2.5) and (2.6),

$$L \begin{bmatrix} \frac{di_{La}}{dt} \\ \frac{di_{Lb}}{dt} \\ \frac{di_{Lc}}{dt} \end{bmatrix} = \begin{bmatrix} u_{La} \\ u_{Lb} \\ u_{Lc} \end{bmatrix} - \begin{bmatrix} u_a \\ u_b \\ u_c \end{bmatrix} \tag{2.7}$$

$$C\begin{bmatrix}\frac{du_a}{dt}\\ \frac{du_b}{dt}\\ \frac{du_c}{dt}\end{bmatrix}=\begin{bmatrix}i_{La}\\ i_{Lb}\\ i_{Lc}\end{bmatrix}-\begin{bmatrix}i_a\\ i_b\\ i_c\end{bmatrix} \tag{2.8}$$

The equation (2.7) and (2.8) are the amount of change in the mathematical model of the three-phase inverter over time in the abc stationary reference frame, although this model is relatively intuitive but not conducive to designing the control system. Therefore, the stationary reference frame is converted into a synchronously rotating reference frame to keep it synchronized with the fundamental frequency[14].

With the abc – dq transformation matrix

$$T_{abc\to dq}=\frac{2}{3}\begin{bmatrix}sin\omega t & \sin(\omega t-\frac{2\pi}{3}) & \sin(\omega t+\frac{2\pi}{3})\\ cos\omega t & \cos(\omega t-\frac{2\pi}{3}) & \cos(\omega t+\frac{2\pi}{3})\end{bmatrix} \tag{2.9}$$

The equation (2.7) and (2.8) can be rewritten as

$$Ls\begin{bmatrix}i_{Ld}\\ i_{Lq}\end{bmatrix}=\begin{bmatrix}u_{Ld}\\ u_{Lq}\end{bmatrix}-\begin{bmatrix}u_d\\ u_q\end{bmatrix}+\omega L\begin{bmatrix}i_{Lq}\\ -i_{Ld}\end{bmatrix} \tag{2.10}$$

$$Cs\begin{bmatrix}u_d\\ u_q\end{bmatrix}=\begin{bmatrix}i_{Ld}\\ i_{Lq}\end{bmatrix}-\begin{bmatrix}i_d\\ i_q\end{bmatrix}+\omega C\begin{bmatrix}u_q\\ -u_d\end{bmatrix} \tag{2.11}$$

Thus, the microgrid inverter mathematic model can be shown as equation (2.10) and (2.11).

2.3 Droop Control

2.3.1 Background

The stability of the power system has always been an important criterion for measuring the quality of the power system. However, due to the wide application of renewable energy in the microgrid, the stability and reliable operation of the grid has been affected. Droop control is a good control method for enhancing the stability of power systems dominated by grid-connected inverters.

The droop control is to calculate the output power of the microgrid power supply outlet voltage and current and use the set droop characteristic curve to convert the power into a control signal with the output voltage frequency and amplitude as the command. The power is reversed to the output voltage signal, and finally the load power can be reasonably distributed, and the voltage and frequency of the microgrid power output can also be stabilized[15].

2.3.2 Introduction

For only one inverter (Figure2.5), the active power and the reactive power delivered by the source to the terminal through the impedance can be obtained as following [16][17]

$$P = \left(\frac{EV_0}{Z_0}cos\delta - \frac{V_0^2}{Z_0}\right)cos\theta + \frac{EV_0}{Z_0}sin\delta sin\theta \tag{2.12}$$

$$Q = \left(\frac{EV_0}{Z_0}cos\delta - \frac{V_0^2}{Z_0}\right)sin\theta - \frac{EV_0}{Z_0}sin\delta cos\theta \tag{2.13}$$

Where, δ is the power angle.

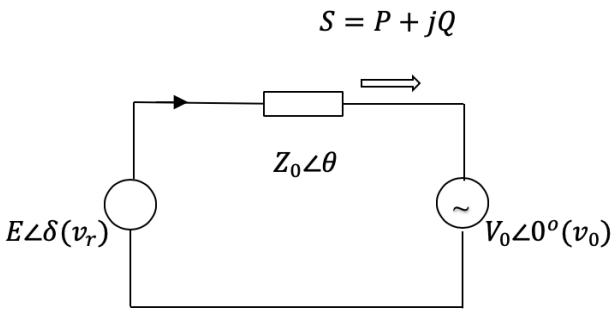

Figure 2.5 Power delivered to a voltage source through an impedance

For two inverters operated in parallel (Figure 2.6)

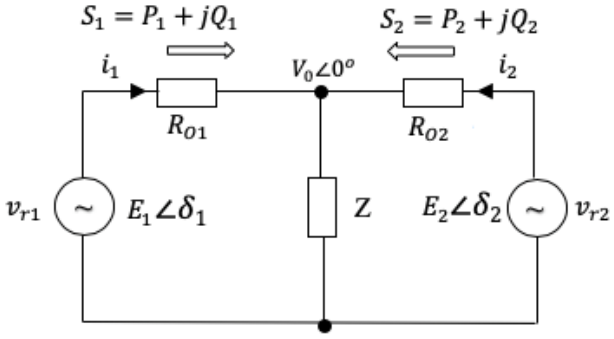

Figure 2.6 Two inverters operated in parallel

The complex power of the inverter output is

$$\widetilde{S_i} = P_i + jQ_i = 3\dot{V}\dot{I}_i^* = 3(\frac{V}{\sqrt{2}}\angle 0)(\frac{\frac{V_i}{\sqrt{2}}\angle\delta_i - \frac{V}{\sqrt{2}}\angle 0}{Z_i\angle\theta_i})^* \tag{2.14}$$

The active and reactive power of the inverter output is

$$P_i = \frac{3}{2}\frac{V}{R_i^2+X_i^2}[R_i(V_i cos\delta_i - V) + X_i V_i sin\delta_i] \quad (2.15)$$

$$Q_i = \frac{3}{2}\frac{V}{R_i^2+X_i^2}[-R_i V_i sin\delta_i + X_i(V_i cos\delta_i - V)] \quad (2.16)$$

Table 2.1 shows the transmission line impedance parameters used in a typical microgrid system.[18]

Table 2.1 Impedance parameters of typical transmission lines

Type of line	R (Ω/km)	X (Ω/km)	I_N(A)	R/X
Low voltage	0.642	0.083	142	7.7
Medium voltage	0.616	0.190	396	0.85
High voltage	0.06	0.191	580	0.31

1) High voltage system power transmission characteristics

In high-voltage systems, the value of reactance is much larger than the resistance value, so the $R_i \approx 0, \theta_i \approx \pi/2$. Then, the equation (2.15) and (2.16) can be rewritten as [16-18]

$$P_i = \frac{3}{2}\frac{VV_i}{X_i} sin\delta_i \quad (2.17)$$

$$Q_i = \frac{3}{2}\frac{V(V_i cos\delta_i - V)}{X_i} \quad (2.18)$$

Then, because$\delta_i \approx 0$, $sin\delta_i = \delta_i, cos\delta_i = 1$

$$P_i = \frac{3}{2}\frac{VV_i}{X_i}\delta_i \quad (2.19)$$

$$Q_i = \frac{3}{2}\frac{V(V_i - V)}{X_i} \quad (2.20)$$

2) Medium voltage system power transmission characteristics

In medium voltage systems, the transmission line impedance is resistive. So the $\delta_i \approx 0$

$$P_i = \frac{3}{2}\frac{V}{R_i^2+X_i^2}[R_i(V_i - V) + X_i V_i \delta_i] \quad (2.21)$$

$$Q_i = \frac{3}{2}\frac{V}{R_i^2+X_i^2}[-R_i V_i \delta_i + X_i(V_i - V)] \quad (2.22)$$

3) Low voltage system power transmission characteristics

In low voltage system, the value of reactance is much smaller than the resistance value. So $X_i \approx 0, \theta_i \approx 0, \delta_i \approx 0$, $sin\delta_i = \delta_i, cos\delta_i = 1$.

$$P_i = \frac{3}{2}\frac{V(V_i - V)}{R_i} \tag{2.23}$$

$$Q_i = -\frac{3}{2}\frac{VV_i}{R_i}\delta_i \tag{2.24}$$

2.3.3 The Principle of Droop Control

When the impedance of the transmission line is inductive, the traditional p-f, q-v droop control can be expressed as [16-18]

$$f = f_n - m(P - P_n) \tag{2.25}$$

$$V = V_n - n(Q - Q_n) \tag{2.26}$$

Where, f and f_n are the actual and rated values of the micropower output voltage frequency. V and V_n are the actual and rated values of the micropower output voltage. P and P_n are the actual values and ratings of the active power output from the micro power supply. Q and Q_n are the actual values and ratings of the reactive power output of the micro power supply, m and n are the droop coefficients of frequency and voltage.

The droop coefficients m and n can be expressed as

$$m = \frac{f_n - f_{min}}{P_{max} - P_n} \tag{2.27}$$

$$n = \frac{V_n - V_{min}}{Q_{max} - Q_n} \tag{2.28}$$

Where, P_{max} is the maximum value of the active power output, f_{min} is the minimum voltage frequency allowed when the active power output is maximum, Q_{max} is the maximum value of reactive power output, V_{min} is the minimum voltage allowed when the reactive power output is maximum.

When the impedance of the transmission line is resistive, the traditional p-f, q-v droop control can be expressed as

$$f = f_n + n(Q - Q_n) \tag{2.29}$$

$$V = V_n - m(p - p_n) \tag{2.30}$$

The p-f, q-v droop control characteristic curve is shown in the Figure 2.7, assuming that the initial operating point of the micro power supply is the equilibrium point A. When the active power of the system load increases, the output active power of the micro power supply is as shown in Figure a, and the balance point changes from A to B and the frequency decreases to f_{min}. When the reactive power of the load of the system increases, the reactive power output by

the micro power supply at this time is as shown in Figure 2.7. And the balance point changes from A to B, and the voltage drops to V_{min}. Therefore, to achieve stable output voltage and frequency of the micro power supply, it is necessary to set reasonable droop control parameters.

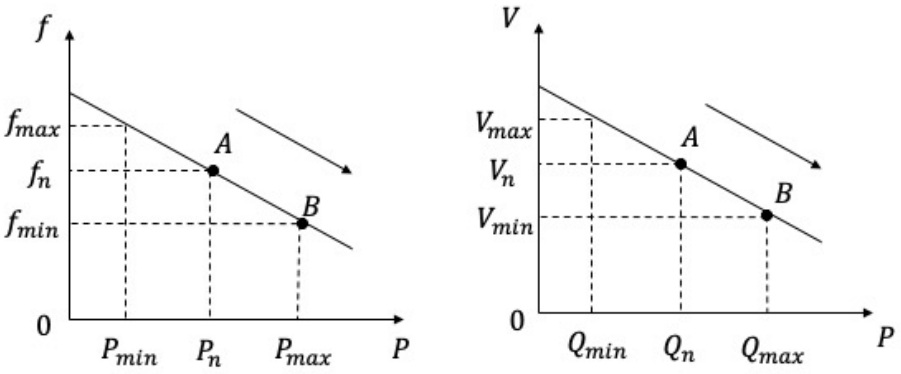

Figure 2.7 Droop control characteristic curve

2.3.4 The Design of Droop Control

In microgrid, distributed power supplies typically require an energy storage device to supply power to the load when necessary. Assume that the DC side capacitor voltage V_{DC} of the inverter remains substantially unchanged.

In Figure 2.8, the inverter circuit consisting of voltage source inverters uses PWM modulation, L_{abc}, C_{abc} and R_{abc} are three-phase filter inductors, capacitors and impedances, Z_{abc} is the three-phase load impedance and is connected to the distribution line. R'_{abc} and L'_{abc} is the line resistance and inductance. i_{Labc} is the output current of the inverter, i_{Cabc} is the filter capacitor current, and i_{Zabc} is the load current.

The structure diagram of the controller is shown by the dashed box in the Figure 2.8. The design of droop control in this thesis paper contains three parallel inverters, each of which contains a power calculation block, a voltage and current double loop control block, and a droop control block. The signal obtained by the double loop control block is input to the PWM, and the inverter thyristor is driven to be disconnected to realize the microgrid inverter control. The structure of droop control is shown in Figure 2.8.

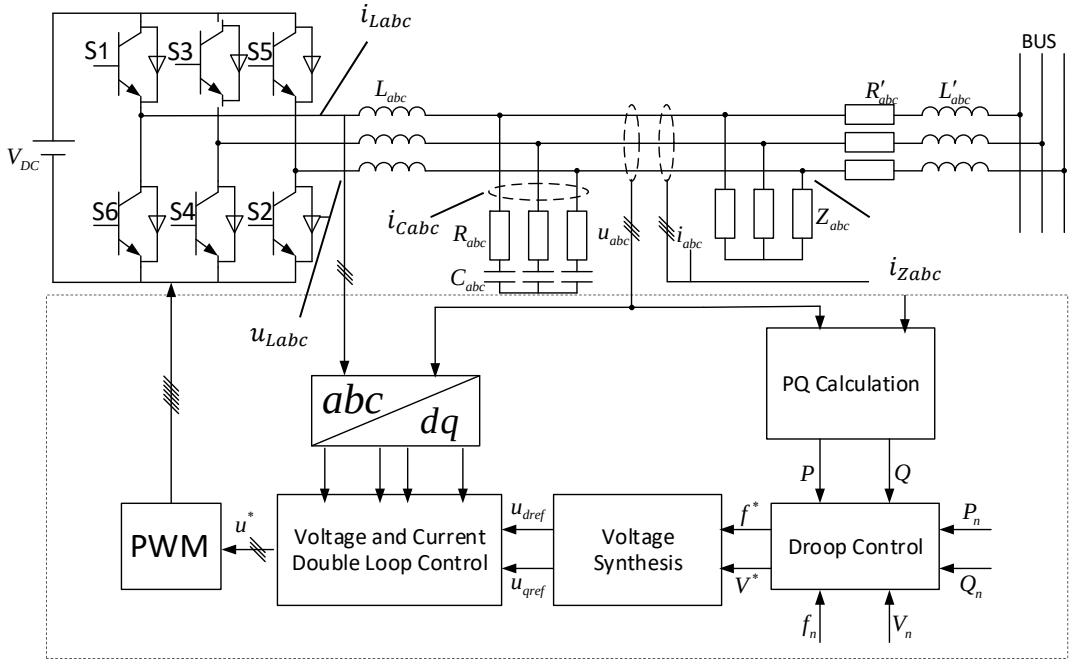

Figure 2.8 The structure of droop control

2.3.5 Power Transmission Block Parameter Design

The power calculation in the power control block can calculate the instantaneous active and reactive power on the transmission line according to the instantaneous voltage and current values collected by the sensor [16-18].

$$p = u_a i_a + u_b i_b + u_c i_c \tag{2.31}$$

$$q = \frac{1}{\sqrt{3}}(u_{bc} i_a + u_{ca} i_b + u_{ab} i_c) \tag{2.32}$$

Converting instantaneous active power and reactive power from abc stationary coordinate system to dq rotating coordinate system can get,

$$p = \frac{3}{2}(u_d i_d + u_q i_q) \tag{2.33}$$

$$q = \frac{3}{2}(u_q i_d - u_d i_q) \tag{2.34}$$

In order to eliminate the harmonic components in the instantaneous power, the instantaneous active power and the reactive power need to be filtered by the first-order low-pass filter to obtain the fundamental active power and reactive power, which are used as the input power of the droop control link.

$$P = \frac{\omega_c}{s+\omega_c} p \tag{2.35}$$

$$Q = \frac{\omega_c}{s+\omega_c} q \tag{2.36}$$

From the above equations, the structure of power controller can be got (Figure 2.9).

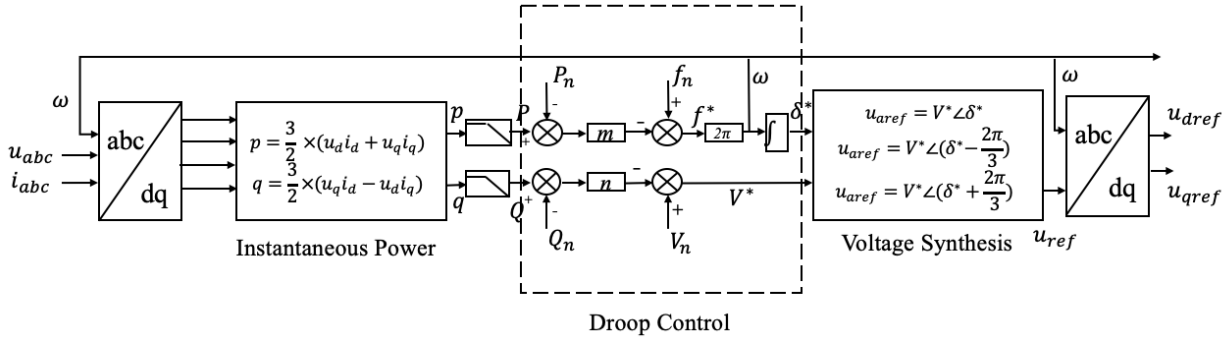

Figure 2.9 The structure of power controller

2.3.6 Voltage and Current Double Loop Parameter Design

The voltage and current double loop control use an outer voltage loop and an inner current loop. As shown in the Figure 2.10, in order to improve the steady-state accuracy of the output voltage amplitude and frequency, the outer voltage loop uses proportional integral (PI) control, the outer voltage loop proportional coefficient is K_{uP}, and the integral coefficient is K_{uI}. In the design of the inner current loop, the main consideration is to enhance the dynamic response speed and reduce the time to reach the steady state. Proportional control is used here, where the proportional coefficient is K_{iP}. The inverter thyristor adopts PWM technology and the transfer function value is K_{PWM}.[16-18]

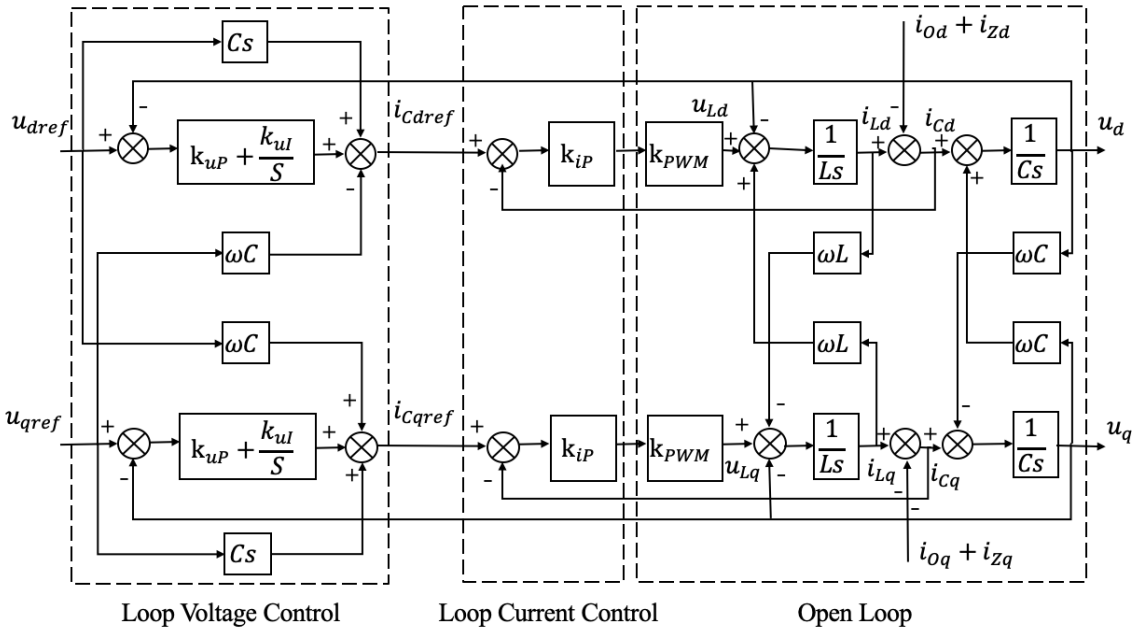

Figure 2.10 Voltage and current double loop

Taking i_{Cdref} as the input and i_{Cd} as the output, the inner current loop transfer function is

$$i_{Cd} = \frac{k_{iP}k_{PWM}Cs}{LCs^2+k_{iP}k_{PWM}Cs+1} i_{Cdref} - \frac{LCs^2}{LCs^2+k_{iP}k_{PWM}Cs+1}(i_{Od} + i_{Zd}) \tag{2.37}$$

The transfer function of the current proportional gain can be obtained as follows

$$G_i(s) = \frac{k_{iP}k_{PWM}Cs}{LCs^2+k_{iP}k_{PWM}Cs+1} \tag{2.38}$$

The equivalent output impedance of the current loop is

$$Z_i(s) = \frac{LCs^2}{LCs^2+k_{iP}k_{PWM}Cs+1} \tag{2.39}$$

Taking u_{dref} as the input and u_d as the output, the outer voltage loop transfer function is

$$i_{Cdref} = (u_{dref} - u_d)(k_{uP} + \frac{k_{uI}}{s}) + u_{dref}Cs \tag{2.40}$$

Combine the equation (2.40) and (2.37), can get

$$u_d = G_u(s)u_{dref} - Z(s)(i_{Od} + i_{Zd}) \tag{2.41}$$

Voltage proportional gain transfer function is

$$G_u(s) = \frac{k_{iP}k_{PWM}Cs^2+k_{iP}k_{PWM}k_{uP}s+k_{iP}k_{PWM}k_{uI}}{LCs^2+k_{iP}k_{PWM}Cs^2+(1+k_{iP}k_{PWM}k_{uP})s+k_{iP}k_{PWM}k_{uI}} \tag{2.42}$$

The equivalent output impedance of the inverter is

$$Z(s)=\frac{Ls^2}{LCs^2+k_{iP}k_{PWM}Cs^2+(1+k_{iP}k_{PWM}k_{uP})s+k_{iP}k_{PWM}k_{uI}} \tag{2.43}$$

From the equation (2.43), the equivalent output impedance of the inverter will be affected by the main circuit parameters of the inverter and will also be affected by the parameters of the voltage and current double loop control module.

Then the characteristic equation of the control system is

$$s^3+\frac{k_{iP}k_{PWM}}{L}s^2+\frac{1+k_{iP}k_{PWM}k_{uP}}{LC}s+\frac{k_{iP}k_{PWM}k_{uI}}{LC} \tag{2.44}$$

Assume that the closed-loop expected pole of the control system is

$$s_{1,2}=-\xi\omega_r\pm j\omega_r\sqrt{1-\xi^2} \tag{2.45}$$

$$s_3=-a\xi\omega_r \tag{2.46}$$

Where ξ is expected damping ratio, ω_r is natural oscillation frequency.

Then the expected characteristic equation of current-voltage double-loop control is

$$D(s)=(s-s_1)(s-s_2)(s-s_3)=(s^2+2\xi\omega_r s+{\omega_r}^2)(s+a\xi\omega_r) \tag{2.47}$$

Then

$$k_{iP}=\frac{\xi\omega_r(2+a)L}{k_{PWM}} \tag{2.48}$$

$$k_{uP}=\frac{{\omega_r}^2(1+2a\xi^2)LC-1}{k_{iP}k_{PWM}} \tag{2.49}$$

$$k_{uI}=\frac{a\xi{\omega_r}^3LC}{k_{iP}k_{PWM}} \tag{2.50}$$

The design parameters in this thesis paper are

Table 2.2 Parameter of voltage and current double loop

V_{DC}/V	L/mH	$C/\mu F$	R/Ω	ξ	ω_r	a
800	1	500	0.01	0.8	2500	10

Then the proportional integral parameter of the double loop control can be obtained as

$$\begin{cases} k_{iP}=0.06 \\ k_{uP}=1.7552 \\ k_{uI}=2604.166 \end{cases} \tag{2.51}$$

According to the calculation results, the frequency domain response curve of the equivalent output impedance of the inverter $Z(s)$ can be obtained by MATLAB simulation.

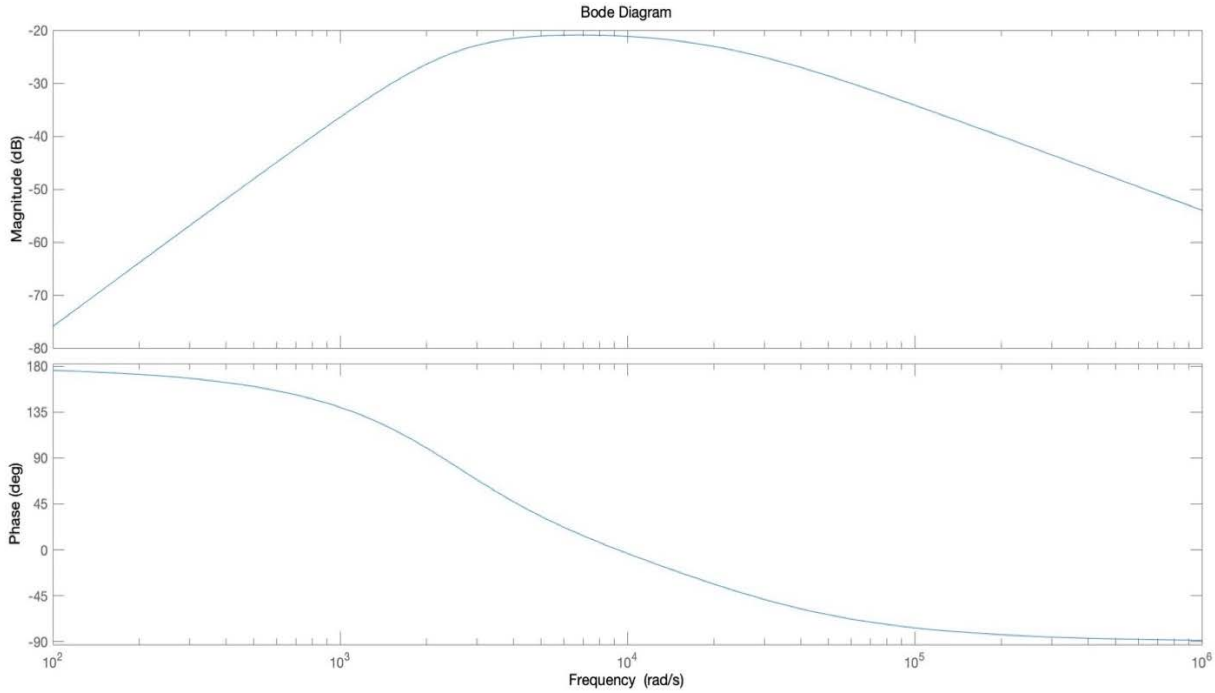

Figure 2.11 Frequency characteristics of $Z(s)$

From the Figure 2.11, the equivalent output impedance of the inverter is resistive at a frequency of 60 Hz (376.99 rad/s). In order for the inverter to meet the control characteristics of the traditional droop control, it is necessary to re-adjust the double loop control parameters so that the equivalent output impedance of the inverter is inductive near 60 Hz (376.99 rad/s).

Keep the proportional coefficient k_{uP} and integral coefficient k_{uI} of the voltage loop unchanged. When the proportional coefficient of the current loop k_{iP} increases from 0.001 to 1000, the current loop equivalent impedance frequency domain response curve is shown in Figure 2.12. From the Figure 2.12, as the current loop proportional coefficient increases, the current loop output impedance gradually changes from resistive to inductive. When the value of k_{iP} is 5, the control effect is more ideal.

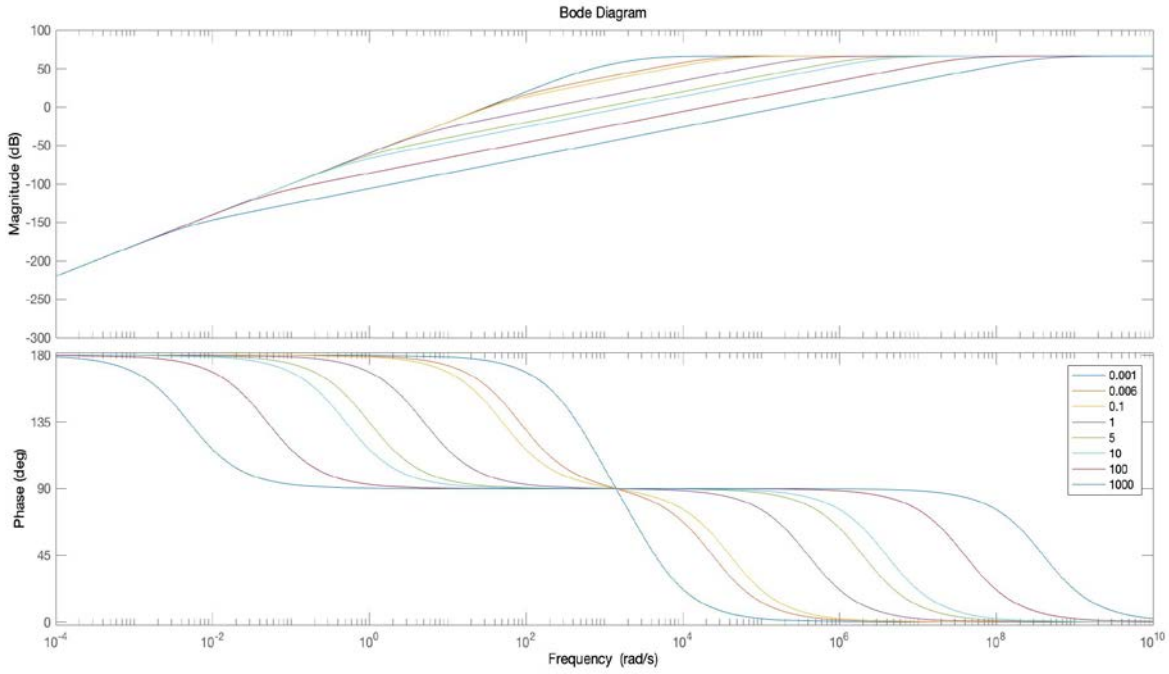

Figure 2.12 Frequency characteristics of $Z_i(s)$ (change k_{iP})

The current loop proportional coefficient k_{iP} is selected to be 5, and the voltage loop proportional coefficient k_{uP} is unchanged. The voltage loop integral coefficient k_{uI} is increased from 1 to 10000. The frequency domain response curve of the inverter equivalent output impedance is shown in Figure 2.13. From the Figure 2.13, when the voltage loop integral coefficient k_{uI} increases, the inverter equivalent output impedance gradually changes from resistive to inductive. When the value of k_{uI} is 100, the control effect is more ideal.

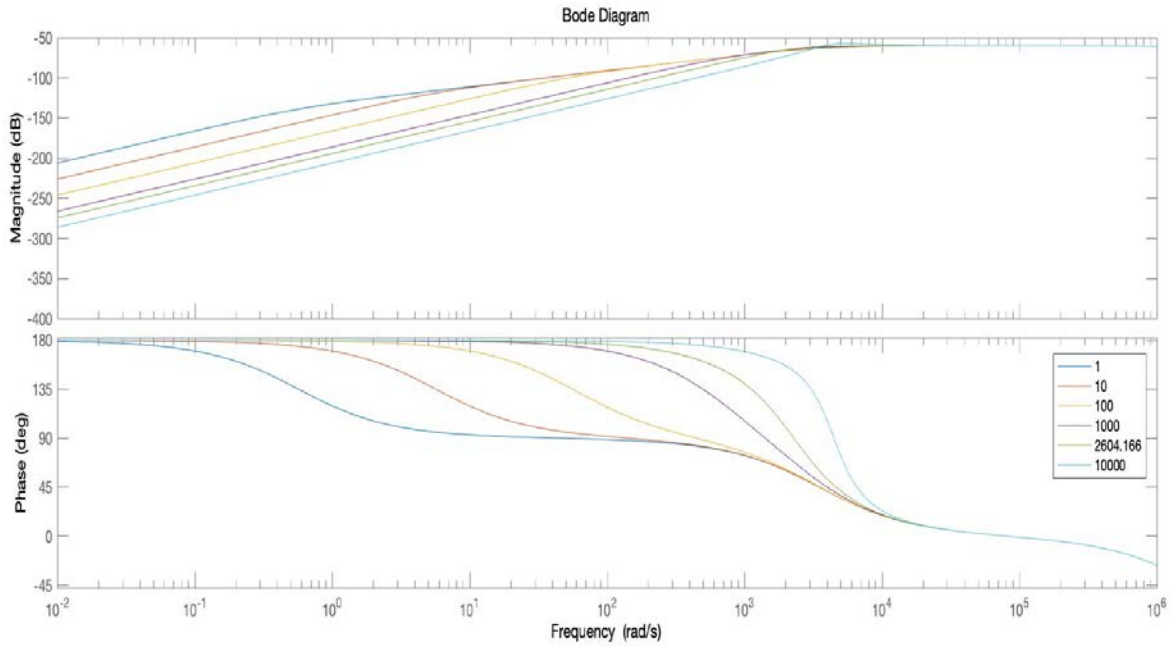

Figure 2.13 Frequency characteristics of $Z(s)$ (change k_{uI})

The current loop proportional coefficient k_{iP} is selected to be 5, and the voltage loop integral coefficient k_{uI} is elected to be 100. The voltage loop proportional coefficient k_{uP} is increased from 0.1 to 100. The frequency domain response curve of the inverter equivalent output impedance is shown in Figure 2.14. When the voltage loop proportional coefficient k_{uP} increases, the inverter equivalent output impedance gradually changes from resistive to inductive. Therefore, the voltage loop proportional coefficient k_{uP} can be taken as 10.

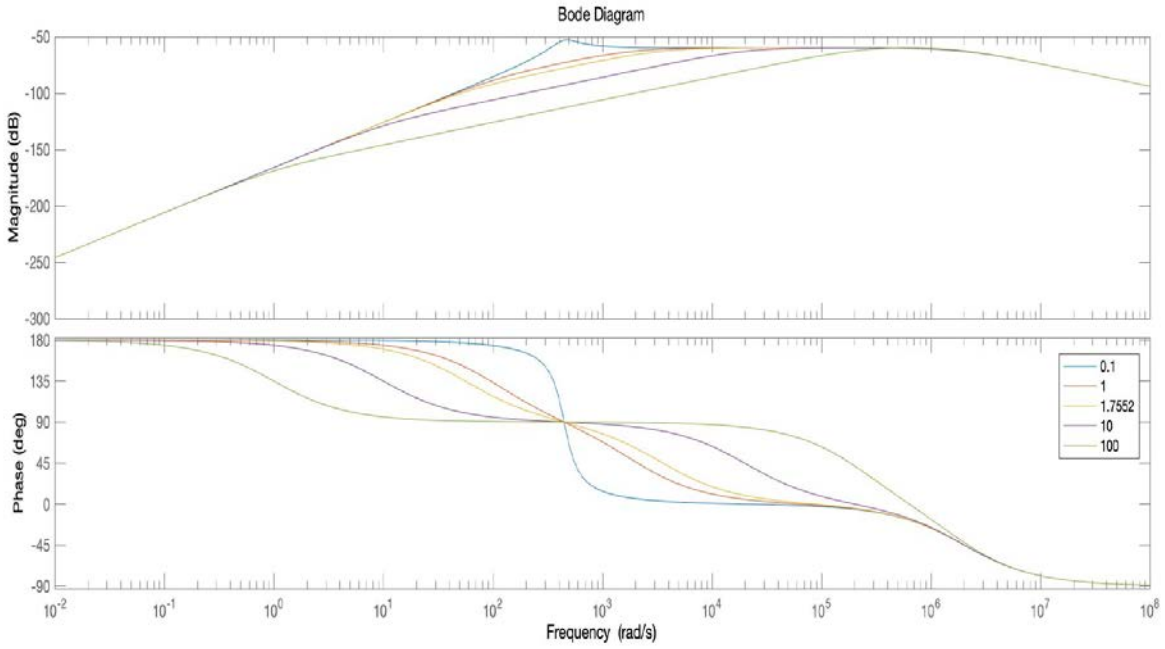

Figure 2.14 Frequency characteristics of $Z(s)$ (change k_{uP})

Then the proportional integral parameter of the double loop control can be obtained as

$$\begin{cases} k_{iP} = 5 \\ k_{uP} = 10 \\ k_{uI} = 100 \end{cases} \tag{2.52}$$

The frequency characteristics of $Z(s)$ with parameter adjusted is shown in Figure 2.15. From Figure 2.15, the output impedance of the inverter is approximately inductive at a frequency of 60 Hz (376.99 rad/s), in accordance with the traditional droop control characteristics.

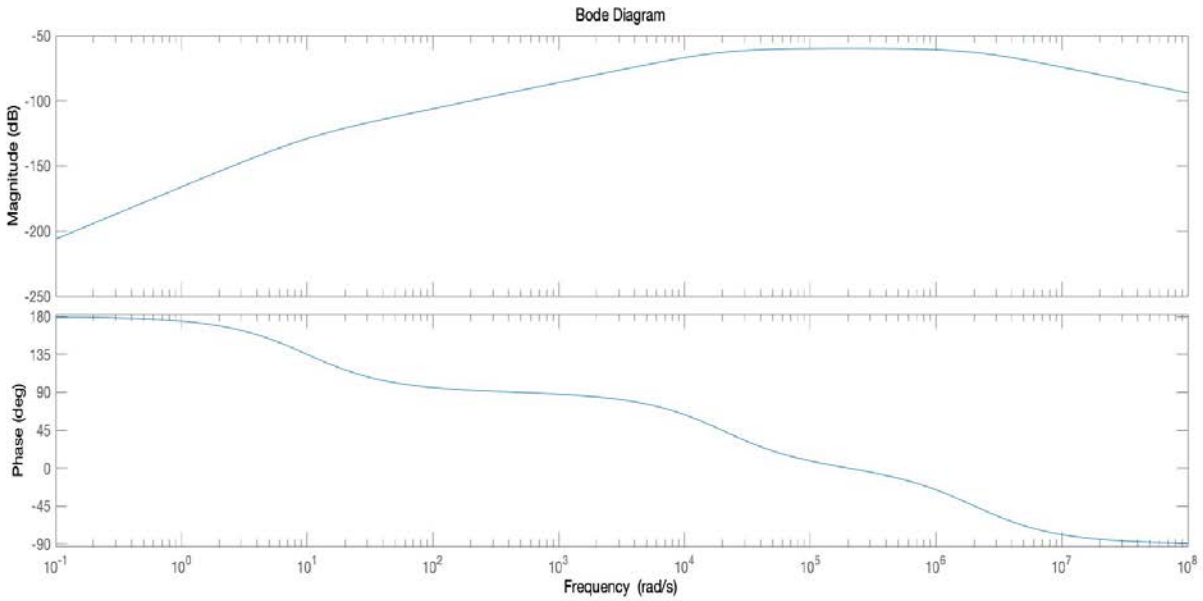

Figure 2.15 Frequency characteristics of $Z(s)$ with parameter adjusted

After adjusting the parameters, the frequency domain response curve of the system voltage proportional gain $G_u(s)$ is shown in Figure 2.16. Figure 2.16 shows that after adjusting the parameters, the system output impedance is guaranteed to be inductive, while ensuring the system's rapidity and stability.

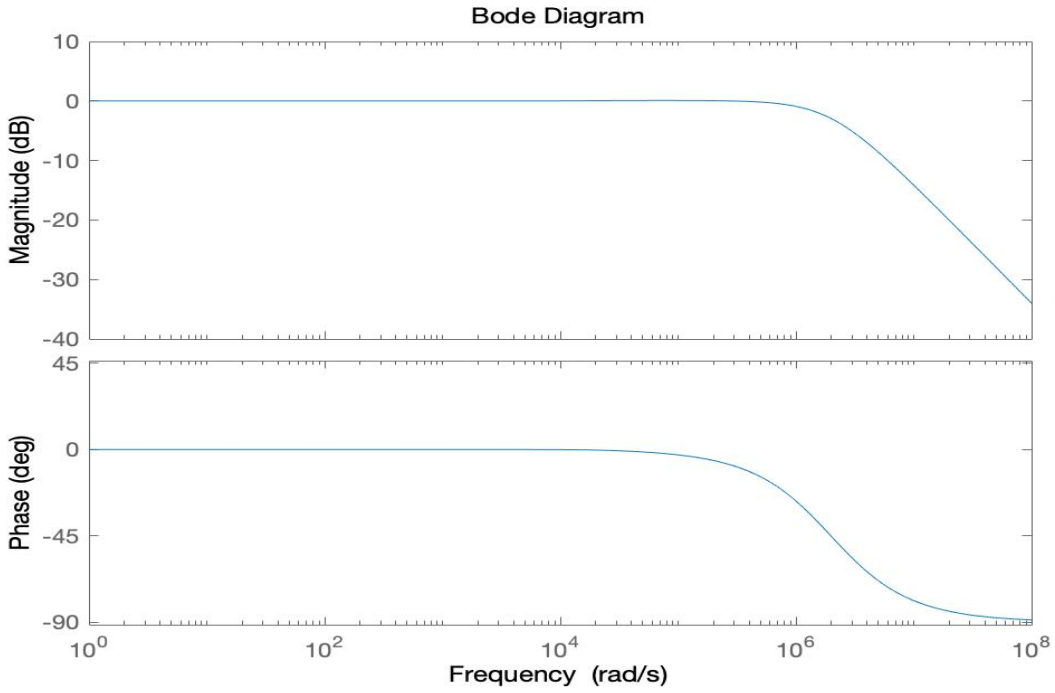

Figure 2.16 Frequency characteristics of $G_u(s)$

2.3.7 The Results of Droop Control

After designing the inverter output impedance to be inductive, the droop characteristics of the conventional high-voltage power system are applied to the low-voltage microgrid. The droop characteristic equations used in this paper are shown in chapter 2.3.3.

The design parameters of this thesis paper are shown in the following Table 2.3

Table 2.3 Parameters of droop control model

	P(kW)	Q(kVar)	m_i	n_i
DG1	80	50	1×10^{-5}	1.2×10^{-5}
DG2	70	40	1×10^{-5}	1.2×10^{-5}
DG3	60	30	1×10^{-5}	1.2×10^{-5}
$V_n = 240V, f_n = 60Hz, k_{uP} = 10, k_{uI} = 100, k_{iP} = 5$				

The results are shown in Figure 2.17 to Figure 2.20.

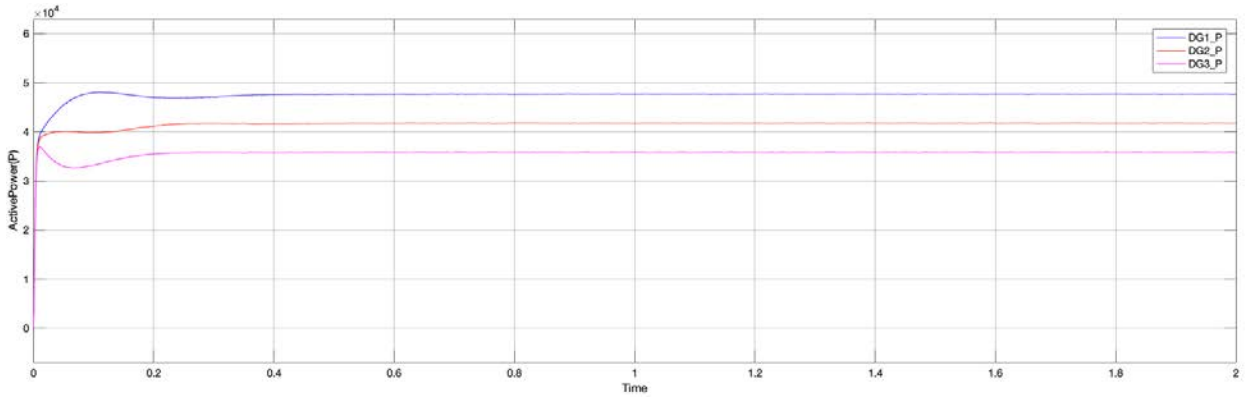

Figure 2.17 The active power ($m_i = 1 \times 10^{-5}$,$n_i = 1.2 \times 10^{-5}$)

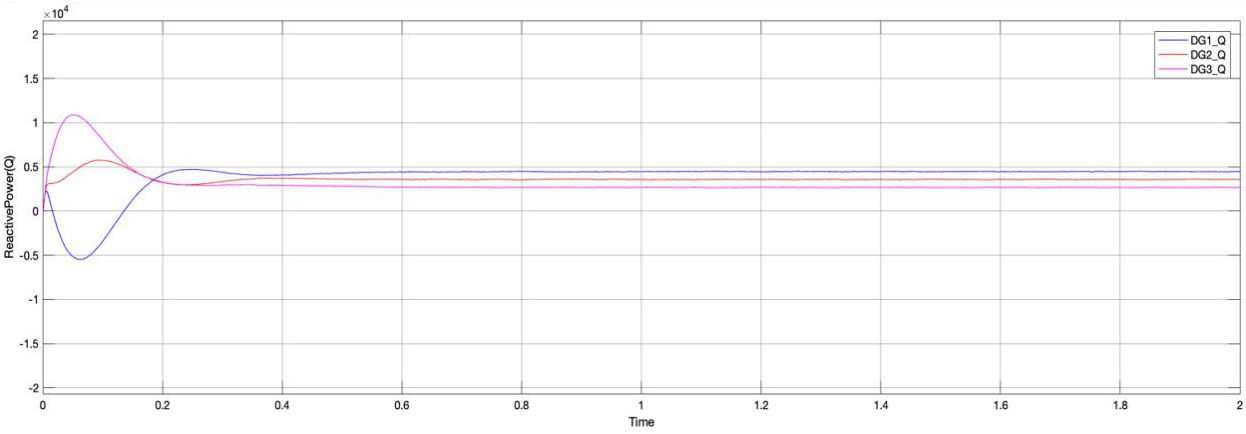

Figure 2.18 The reactive power ($m_i = 1 \times 10^{-5}$,$n_i = 1.2 \times 10^{-5}$)

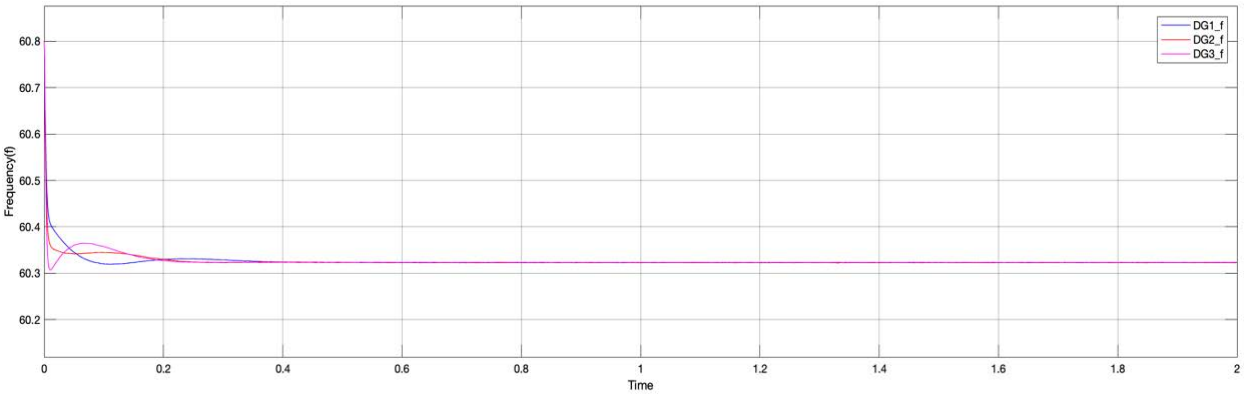

Figure 2.19 The frequency ($m_i = 1 \times 10^{-5}$,$n_i = 1.2 \times 10^{-5}$)

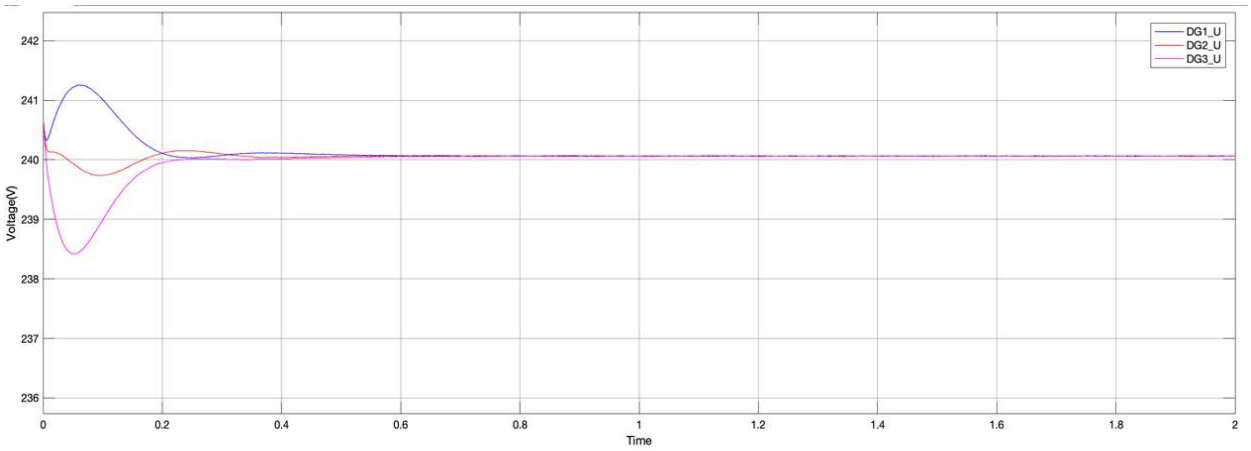

Figure 2.20 The voltage ($m_i = 1 \times 10^{-5}$,$n_i = 1.2 \times 10^{-5}$)

From Figure 2.17 to Figure 2.20, it can be seen that the active power and the reactive power are distributed according to the rated power ratio of the power source. The frequency and voltage are determined by the droop equation.

The initial operation of the microgrid is to assume that load 3 is disconnected from the microgrid. After the initial operation has stabilized, load 3 is connected in parallel with the microgrid at t=0.5. Simulation results are shown in the Figure 2.21 to Figure 2.24.

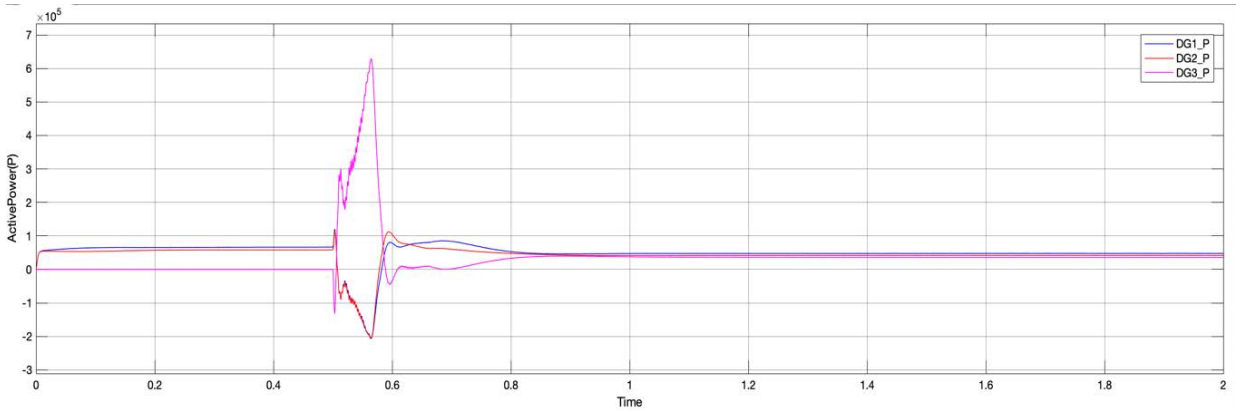

Figure 2.21 The active power (t=0.5 at the disturbance)

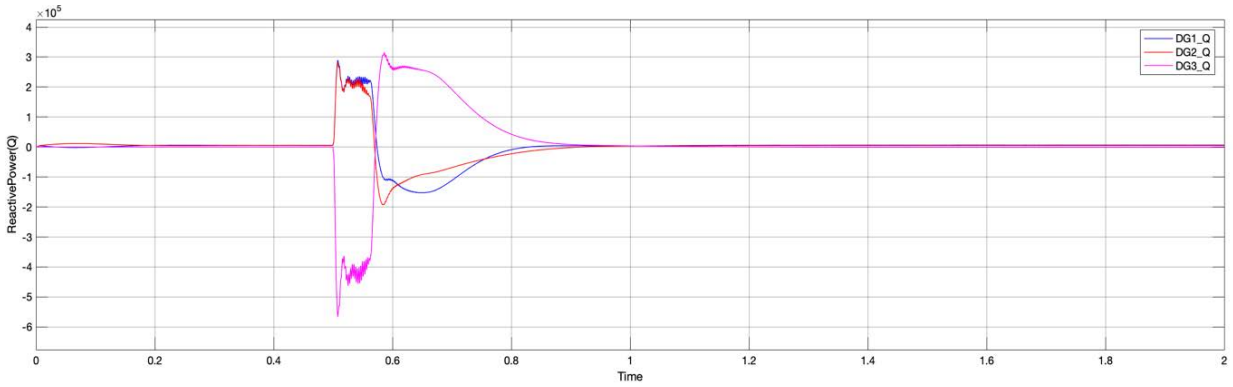

Figure 2.22 The reactive power (t=0.5 at the disturbance)

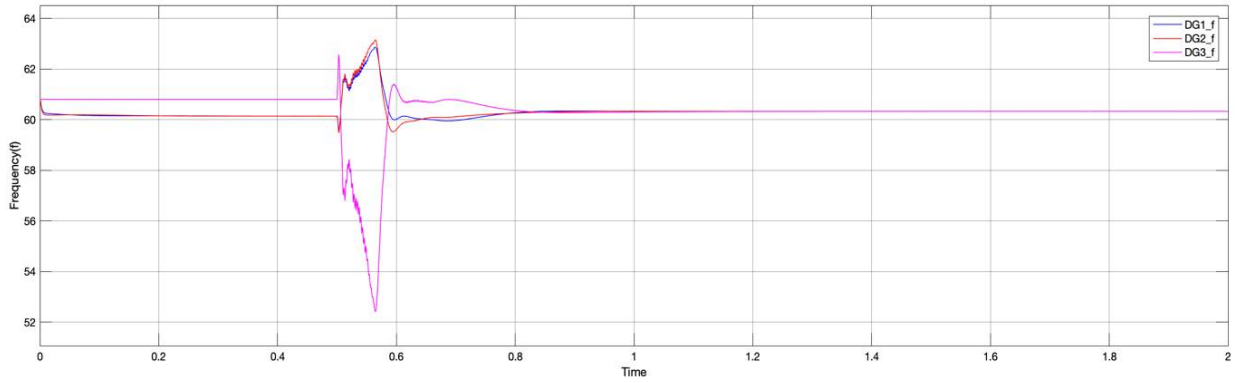

Figure 2.23 The frequency (t=0.5 at the disturbance)

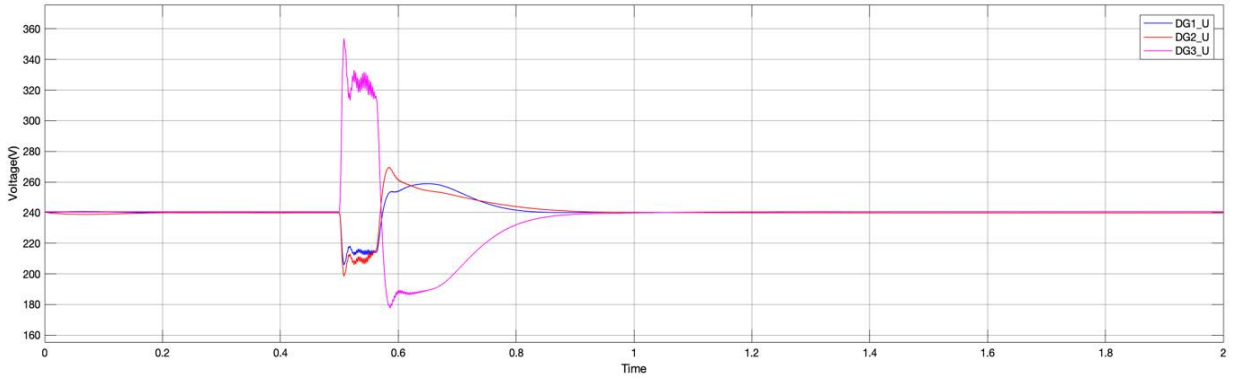

Figure 2.24 The voltage (t=0.5 at the disturbance)

On the basis of the original data, increase the values of m_i and n_i to obtain the following results. (Figure 2.25 to Figure 2.28)

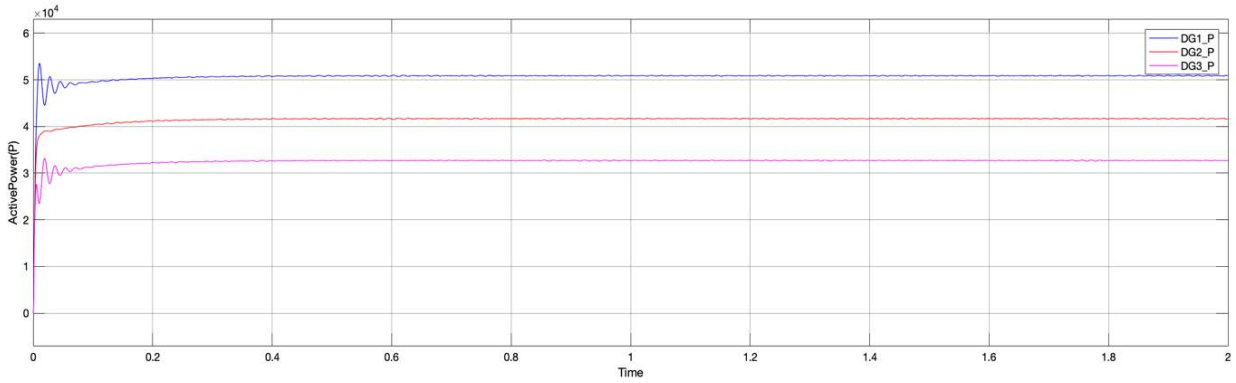

Figure 2.25 The active power ($m_i = 5 \times 10^{-5}$,$n_i = 5.2 \times 10^{-5}$)

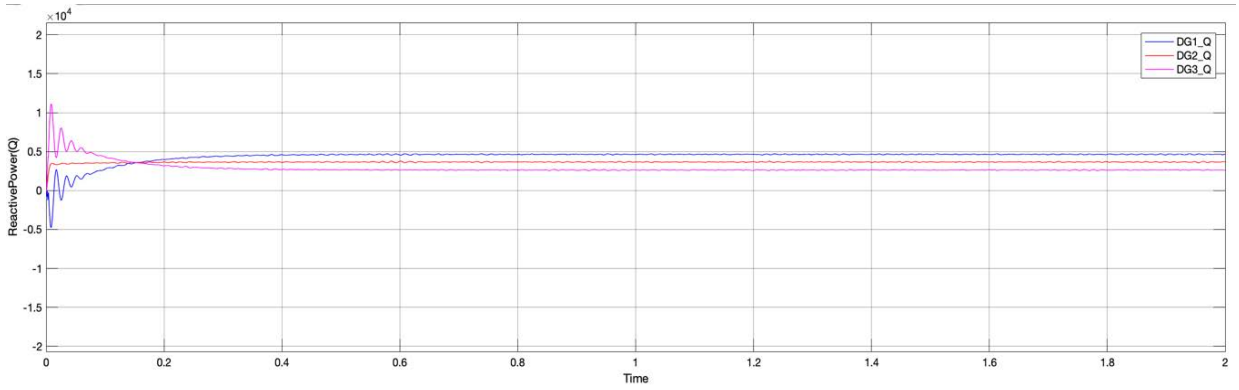

Figure 2.26 The reactive power ($m_i = 5 \times 10^{-5}$,$n_i = 5.2 \times 10^{-5}$)

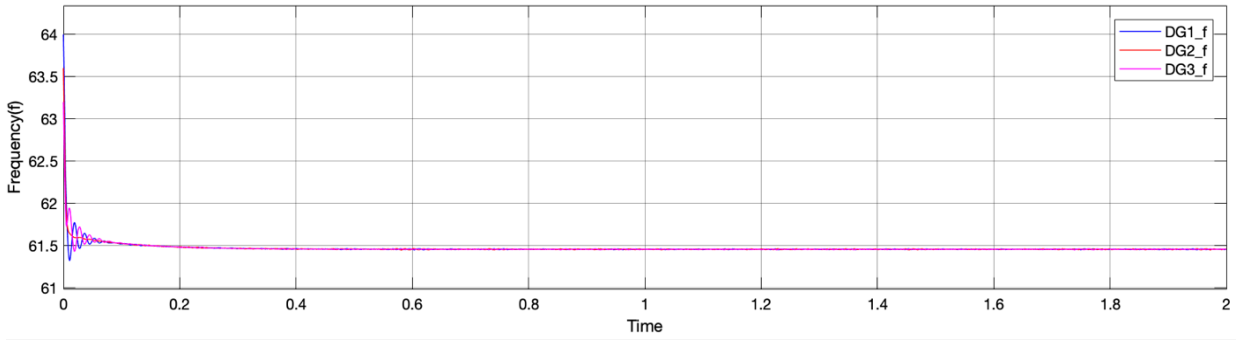

Figure 2.27 The frequency ($m_i = 5 \times 10^{-5}$,$n_i = 5.2 \times 10^{-5}$)

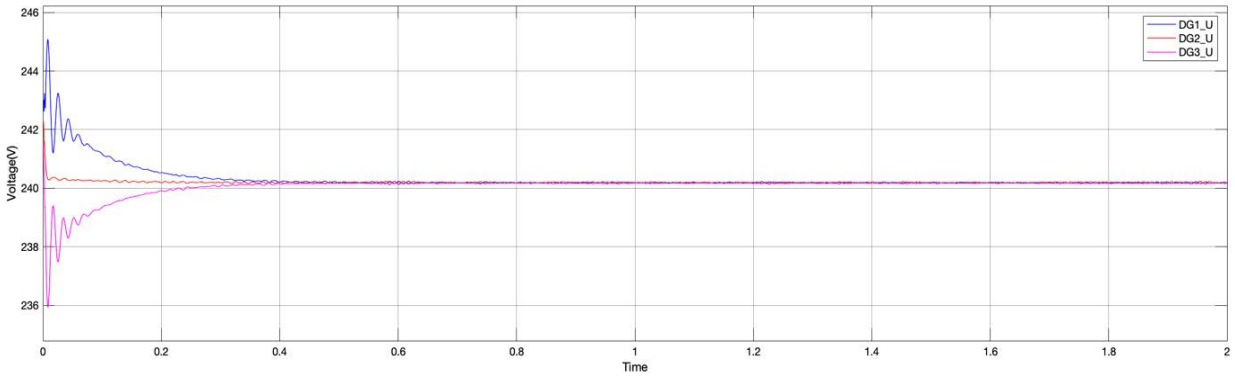

Figure 2.28 The voltage ($m_i = 5 \times 10^{-5}$,$n_i = 5.2 \times 10^{-5}$)

It can be seen from the results that increasing the droop coefficient will increase the fluctuation of the output parameters and cause a large deviation.

2.3.8 The Analysis of The Results of Droop Control

When the droop control strategy is adopted, the output voltage of the inverter can adjust the output of the active power, and the active power will continue to the range frequency, thereby achieving stable frequency adjustment. The adjustment of the voltage amplitude can also be performed in the microgrid. The reactive power realizes the regulation control. In the island microgrid, under the premise of ensuring the stability of the microgrid voltage and frequency, it is also necessary to realize the reasonable distribution of the load power between the microgrid power sources.

1) Frequency stability analysis

In the stable operation state of the microgrid running on the island, it is necessary to meet $m_1 P_{n1} = m_1 P_{n2}$, $f_{n1} = f_{n2}$. In order to achieve the same output frequency of the microgrid power inverter ($f_1 = f_2$), the following conditions must be met

$$m_1 P_1 = m_1 P_2 \tag{2.53}$$

$$m_1 \frac{V_1 V}{X_1} \delta_1 = m_2 \frac{V_2 V}{X_2} \delta_2 \tag{2.54}$$

Assume $\delta_1 = \delta_2, V_1 = V_2,$

Then

$$\frac{m_1}{X_1} = \frac{m_2}{X_2} \tag{2.55}$$

When equation (2.53) is satisfied, the reasonable distribution of the load active power between the microgrid power sources can be achieved, and the output voltage frequency of the inverter will be the same.

2) Voltage amplitude stability analysis

The similar with the frequency stability analysis, in order to ensure that the voltage amplitude of the microgrid power supply output is equal, and the load reactive power is reasonably distributed. Need to meet $\frac{n_1}{X_1} = \frac{n_2}{X_2}$.

However, under actual conditions, when the output power of the microgrid power supply fluctuates too much, the actual output frequency will drop or rise significantly, which will cause instability of the system.

CHAPTER 3. 3D VISUALIZATION DESIGN METHODOLOGY

3D visualization allows people to experience the most real feelings in the virtual reality world, giving people a sense of impressiveness. This chapter focuses on the main methodology of 3D visualization design. This part includes the main design flow, model design method flow, main interface design flow, main environment design flow and animation design method.

3.1 Design Flow Chart

The design of 3D visualization simulation starts with system frame design. The actual images of the various systems in the microgrid such as solar PV, Wind turbine, Energy storage system, microgrid motor control center, etc. are collected. Then, all the microgrid system components are built using 3ds Max software. After that, all the models are imported into the Unity software. The Unity software is then used to create the menu and animation. The simulation design flow chart is shown in Figure.3.1

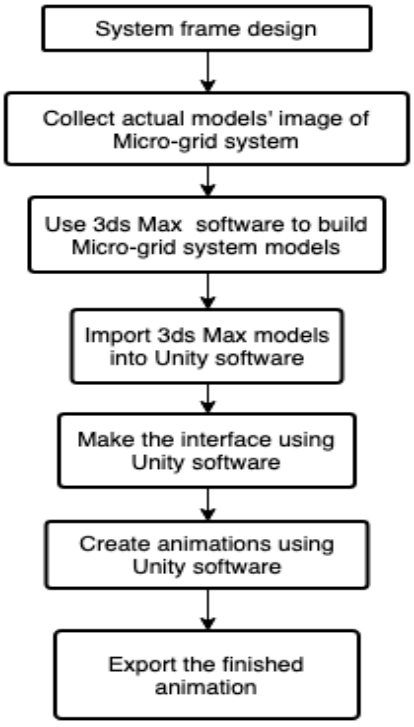

Figure 3.1 Simulation design flow chart

3.2 Basic Model Build Flow

3.2.1 3ds Max Software

3D studio Max (3ds Max), is a professional 3D computer graphics program for making 3D animations, models, games and images. 3ds Max has many important tools for modeling, texture, animation, rendering and dynamics which can meet the requirements of most users. 3ds Max can also be integrated with a variety of related software to provide more operability and diversification [7].

3.2.2 Unity3D Software

Unity3D is a free 3D game engine for designing and building virtual environments. Unity3D software supports three assembly languages: C#, JavaScript, and Boo[5]. The biggest advantage of Unity3D is that it can be designed with a user interface friendly and can handle scenes common in 3d environments, such as terrain, sound, models and animated characters[11]. Unity Graphical User Interface (UGUI) is a powerful User Interface (UI) system that Unity has added in versions 4.6 and above. The UGUI system create a 3D virtual environment setup for demonstrating and administering virtual elements such as virtual objects, text guidance, and audio prompts. These elements are expressed by the UGUI components which define properties such as transform, material, texture etc. UGUI has the advantages of flexibility, visualization, high efficiency, ease of use and expansion[14].

Base on this two software, the basic model build flow is shown in Figure 3.2.

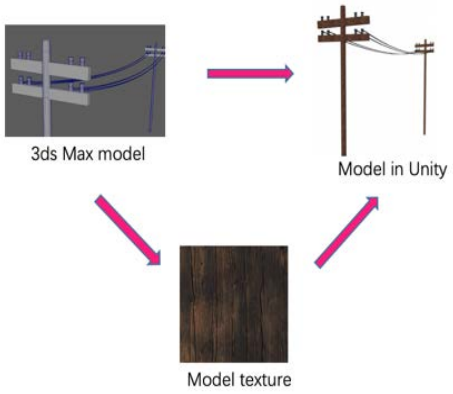

Figure 3.2 Basic model build flow

3.3 Unity Graphical User Interface (UGUI)

To create the User Interface (UI), the UI canvas is created at the beginning. Then, two UI panels including the main menu panel and the introduction panel are designed based on the UI canvas. For the main menu panel, the main menu text and three buttons are built. For the introduction panel, two introduction texts and one button are created. The UGUI system diagram is shown in Figure 3.3.

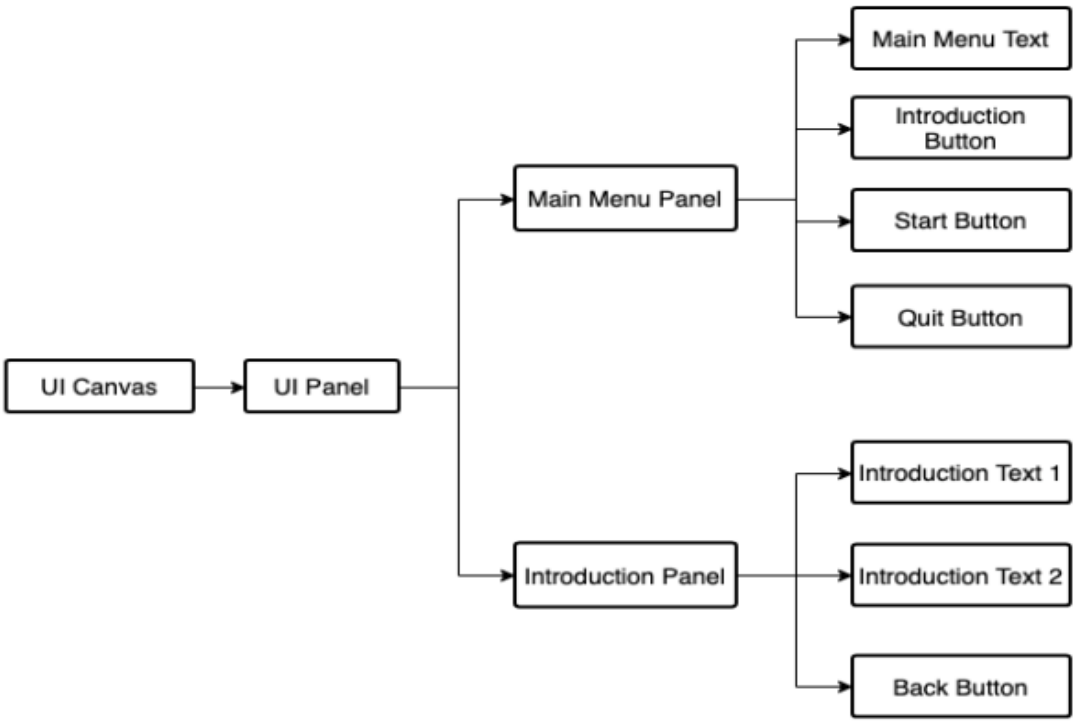

Figure 3.3 The UGUI system diagram

3.4 Terrain Engine

Terrain Engine is selected to increase the environment's realism effect. The external and surrounding virtual model environment are created by using terrain engine in Unity system. It allows designer to ass vast landscape to the virtual environment. The terrain Engine design flow diagram is shown in Figure 3.4.

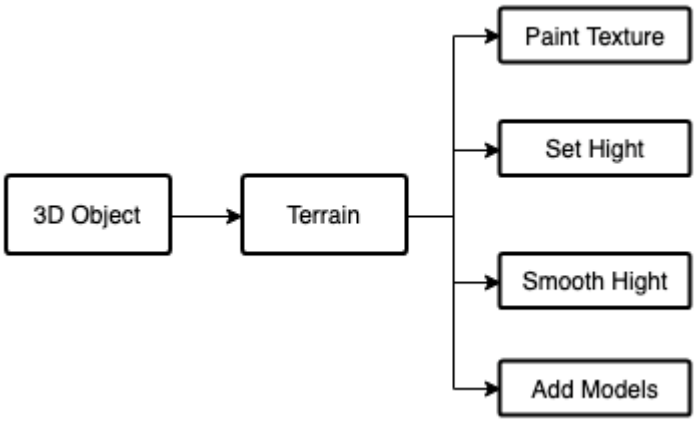

Figure 3.4 The Terrain Engine design flow diagram

3.5 Character Animation

Animation Realization: The animator [22] is plugged into Player Character to implement the cartoon boy animation. Three states are added to cartoon boy, and if the cartoon boy does not move, the animation state will change to “Idle”, if the cartoon boy move, the animation state will change to “Walking (1)”. The state interaction shown in Figure 3.5.

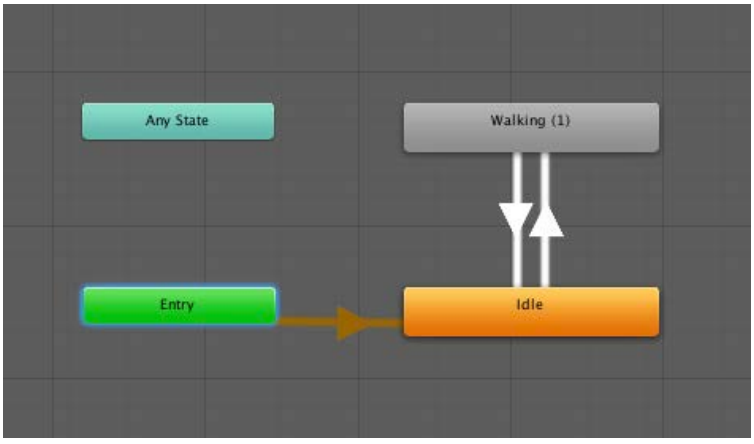

Figure 3.5 Animator state

Collision detection: A set of colliders were created as the boundary of the cartoon boy movement. Events will be triggered whenever cartoon boy touch the colliders. Take the wind turbine boundary collider as an example (shown as green boxes in Figure 3.6).

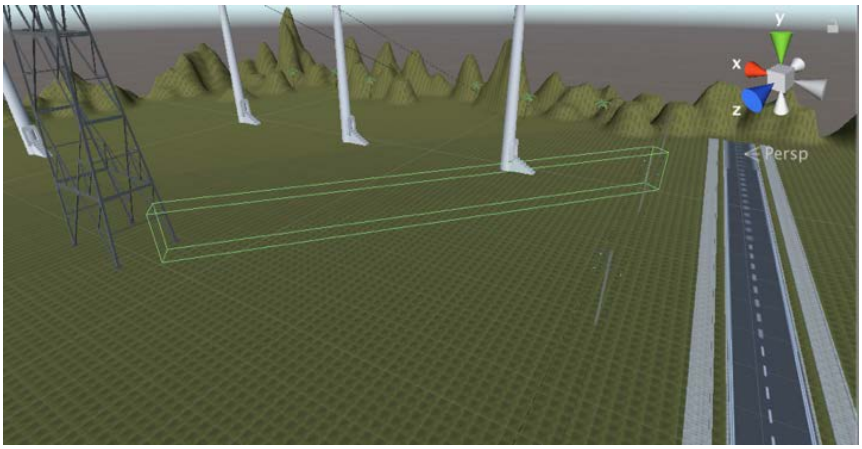

Figure 3.6 Wind turbine boundary collider

CHAPTER 4. 3D VISUALIZATION OF THE MICROGRID

3D visualization of the microgrid is realized by 3ds Max and Unity3D to increase students' interests in Power Engineering. The fundamental model is built through 3ds Max. Then, the Unity3D software is used to create simulation scenarios and define the actions of the character model. In this section, the main components of the designed system will be introduced.

4.1 Friendly Cartoon Character

A friendly cartoon boy model shown in Figure 4.1 with animation component added. The model can be stationary, moving forward or backward or left and right. By choosing a friendly cartoon boy model, can greatly increase the interests of users.

Figure 4.1 Cartoon boy model

4.2 UGUI Menu

User interface design can increase user involvement and create a strong link between the students and the visualization system. This paper also creates a user-friendly interface for students. In the UI system, the main menu provides introduction button, start button and quit button shown in Figure 4.2. User enters the visualization system of the microgrid by clicking the start button. The quit button is to terminate the simulation. The user can click on the introduction button, and then a detailed description of the system model will be displayed, which will make the user more convenient and quicker to understand the system and know how to use it.

Figure 4.2 Main menu

When the user moves the mouse over the button they want to select, the button will be highlighted. Here, the introduction button is used as an example. (Figure 4.3)

Figure 4.3 Highlight button

When the student clicks on the introduction button, it will jump to the introduction panel. Introduction panel provides the introduction of virtual world of microgrid system (Figure 4.4).

Figure 4.4 Introduction

4.3 Microgrid Component – Wind Turbine

4.3.1 Wind Turbine Introduction

Wind power is an important part of renewable energy, and the cost of wind energy is lower than most other energy sources [7], so the use of wind power in the microgrid is becoming more and more popular. Wind turbines are mechanical energy that converts wind energy into useful energy, and the largest possible amount of wind energy is obtained by selecting the number of blades of the appropriate turbine and the speed of rotation. The output power of a wind turbine depends on the speed of the wind. It depends on several important parameters such as air density, aerodynamic disc radius and pitch angle. The generated mechanical torque is calculated by using a mathematical model of the wind turbine [23-25].

4.3.2 Wind Turbine Elements in Unity3D

Cabin: The cabin contains key equipment for the wind turbine, including gearboxes and generators. Maintenance personnel can enter the cabin through the wind turbine tower. The front end of the nacelle is the rotor of the wind turbine, which means the rotor blades and the shaft.

Rotor blades: Catch wind and transmit wind power to the rotor shaft. The design of the blades is very similar to that of an airplane. The materials used are very different, and fibers are used instead of light alloys.

Axis: The rotor axis is attached to the low speed shaft of the wind turbine.

Low speed shaft: The low speed shaft of the wind turbine connects the rotor shaft to the shift gearbox.

Gearbox: The gearbox connects the low-speed and high-speed shafts to increase the speed of the high-speed shaft to 50 times the low-speed shaft.

High-speed shaft and its mechanical brake: The high-speed shaft run at more than 1500 rpm and drives the generator.

Generator: Wind turbine generator converts mechanical energy into electrical energy.

Electronic controllers: One or more computers that constantly monitor the state of the wind turbine are used to control the yaw device.

Hydraulic system: The aerodynamic brake used to reset the wind turbine.

Cooling system: the generator needs cooling when it is running.

Support tower: The wind turbine tower carries the organic cabin and the rotor. A tall tower usually has an advantage because the higher the ground, the greater the wind speed.

Base: The existing base structure includes a straight rod, a tripod and a lattice base.

Anemometer and wind vane: used to measure wind speed and direction.

The Figure 4.5 shows the wind turbine model in this system.

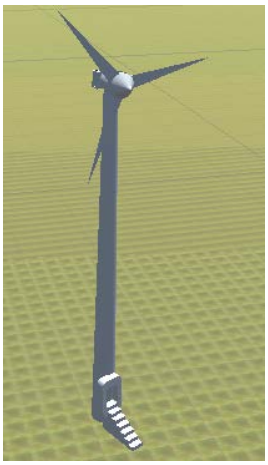

Figure 4.5 Wind turbine model

4.4 Microgrid Component – Solar Panel

4.4.1 Solar Panel Introduction

With the development and progress in the field of power electronics, it has become possible to convert renewable energy into electrical energy. The price of traditional sources of pollution is increasing, and in order to alleviate this expensive energy consumption, microgrids based on renewable energy may be a good substitute, solar energy is a good choice, and governments are also under various plans.

A photovoltaic array is constructed by a series or parallel combination of PV solar cells. The PV cell output voltage is a function of photocurrent, which is primarily determined by the load current, depending on the level of solar radiation during operation. If the temperature and solar radiation levels change, the voltage and current output of the PV array will also change[26][27].

4.4.2 Solar Panel Elements in Unity3D

The solar photovoltaic power generation system is composed of a solar battery pack, a solar controller, and a battery (group).

solar panel: The solar panel is the core part of the solar photovoltaic power generation system. The function of the solar panel is to convert the solar light energy into electrical energy, and the output direct current is stored in the storage battery. Solar panels are one of the most important components in solar photovoltaic systems, and their conversion rate and service life are important factors in determining whether solar cells are useful.

Solar Controller: The solar controller is composed of a dedicated processor CPU, electronic components, a display, a switching power tube, and so on.

Battery: The function of the battery is to store the electrical energy emitted by the solar panel when it is exposed to light and release it when needed.

Inverter: The direct output of solar energy is generally 12VDC, 24VDC, 48VDC. In order to supply electrical energy to 220 VAC appliances, it is necessary to convert the DC power generated by the solar photovoltaic system into AC power, so a DC-AC inverter is required. []

The Figure 4.6 shows the solar panel model in this system.

Figure 4.6 Solar panel model

4.5 Microgrid Component – Load

4.5.1 Load Introduction

Load control and management are key components of the microgrid. It is important to maintain a balance between power generation and load. Microgrid control systems need to constantly evaluate the load and prioritize it to maintain this balance.

The management load within the microgrid can vary from individual customers or groups of customers to specific devices or systems within the client. Since the overall intent of the community microgrid is to provide customers with better power service reliability while increasing efficiency, a single management load must be carefully selected to provide the necessary system flexibility while inconvenience to the customer[28][29][30].

4.5.2 Load Elements in Unity3D

Three loads are built in this thesis work. (Figure 4.7)

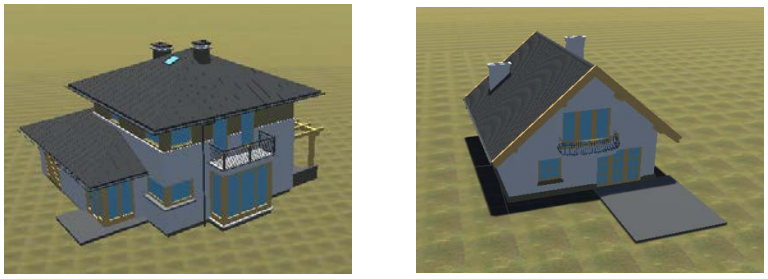

Figure 4.7 Load model

4.6 Microgrid Component – Substation

4.6.1 Substation Introduction

A substation is a key node in the power system network, and a junction for power exchange. It is the system responsible for transmission and distribution between power generation and transmission systems. In order to improve the transmission efficiency and reduce the route loss, when the power plant delivers electric energy to a remote place, it must raise the voltage and turn it into a high-voltage power, and then reduce the voltage according to the demand in the vicinity of the user. Substations play an important role in the reliability performance of power systems. The reliability of a substation to the entire power system can be measured in terms of frequency and duration [31][32].

4.6.2 Substation Elements in Unity3D

There is many electrical equipment involved in a substation system, and they are usually divided into primary equipment and secondary equipment according to their different roles in operation.

Primary equipment refers to the electrical equipment used in the main system of power generation, transmission and distribution. Mainly include generators, transformers, power cables, transmission lines, circuit breakers, disconnectors, transformers, lightning arresters, etc. The utility functions of each device are as follows:

A generator is a mechanical device that converts other forms of energy into electrical energy and is used to produce electrical energy.

When the transformer is in operation, it can transfer the electric energy from its primary side to the secondary side through the conversion of electromagnetic energy, and at the same time, the voltage can be raised or lowered according to the location of the transmission and distribution.

The main functions of power cables: transmission of power, transmission of information, and conversion of electromagnetic energy.

The power transmission line connects the electrical intervals together, and its function is to collect, distribute and transmit electrical energy, so that the power transmission and operation is flexible, and the various electrical equipment connected to the busbar can be inspected and put into operation.

The circuit breaker has a perfect arc extinguishing device and a high-speed transmission mechanism, which can turn on and off the current in the high-voltage circuit under various conditions, and is used to complete the change of the operation mode of the main connection line and to cut off the fault circuit as soon as possible.

The main functions of the isolating switch are isolated power supply, switching operation, and small current.

The secondary equipment refers to the electrical equipment needed to monitor, control, regulate, and protect the working conditions of the primary equipment, and provide the operating personnel with working conditions or production command signals. Mainly include measuring instruments, relays, control and signal devices, automatic devices, etc. This thesis work only gives a model of the primary equipment. (Figure 4.8)

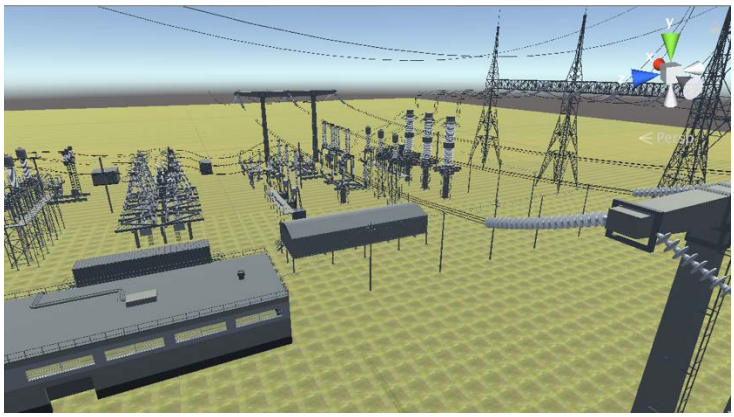

Figure 4.8 Substation model

4.7 Microgrid Component – Energy Storage System (ESS)

4.7.1 Energy Storage System (ESS) Introduction

With the application of renewable energy in microgrid systems, it is becoming more and more important to figure out the intermittent nature of renewable energy and the unstable voltage of the load. The ESS can store power when there is residual energy and readjust it as needed. Therefore, ESS is an important part of the microgrid control system[33][34][35]. Two important factors that affect the capacity and type of ESS components are renewable power profile and the load profile[36].

4.7.2 Energy Storage System (ESS) Elements in Unity3D

The Energy Storage System (ESS) is to ensure the quality of the microgrid power. Among them, the choice of energy storage medium is very important. The lithium battery pack has the advantages of high safety performance, high energy density and fast action speed. Therefore, it becomes the optimal choice for large-capacity energy storage. Figure 4.9. shows Energy Storage System (ESS) models in Unity3D.

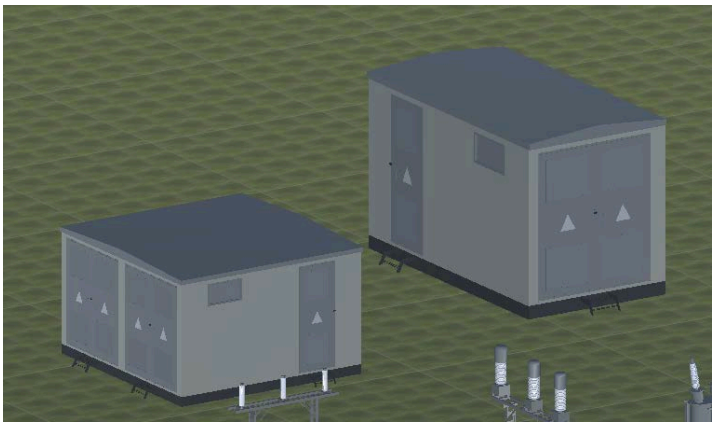

Figure 4.9 Energy Storage System (ESS) model

CHAPTER 5. UNITY3D RESULTS

5.1 Unity Environment

Figure 5.1 shows the 3D visualized microgrid based on Figure 1.2 which including wind turbines, substation, solar panel, transformers, etc. It is clearly showing that the 3D microgrid system is more attractive than the tradition figure shown in Figure1.2. User can also control the perspective of the system through the up, down, left and right keys of the keyboard which makes the user operation more convenient. Students can also imagine themselves as characters in the model and experience the real environment of the microgrid. In this 3D visualized system, students can learn the microgrid components by approaching to these components.

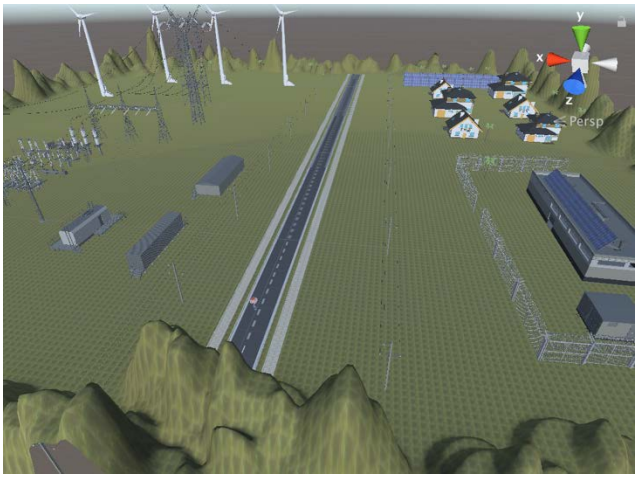

Figure 5.1 3D visualization of the microgrid

Figure 5.2. shows the detailed view of each component in microgrid.

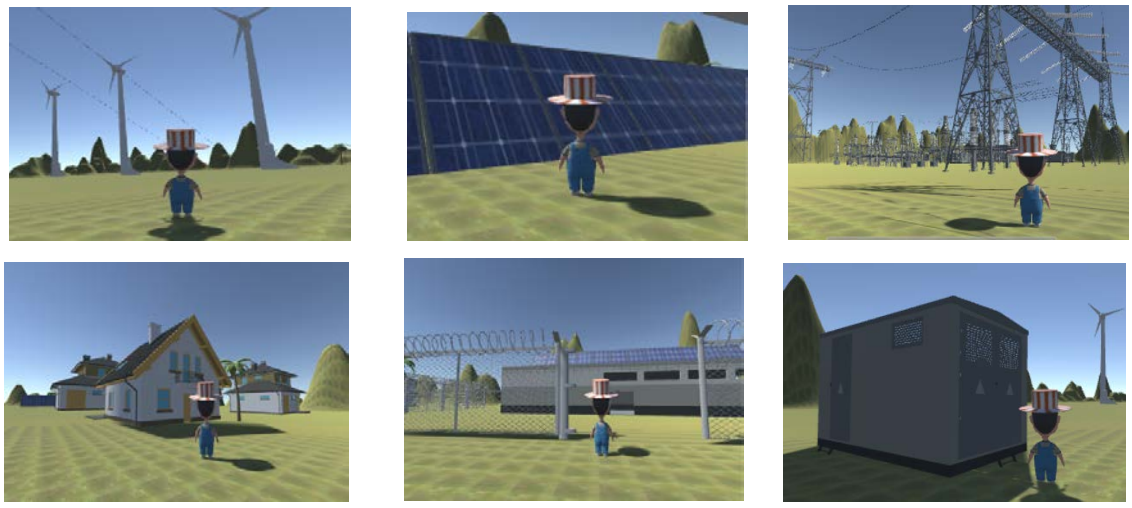

Figure 5.2 The visualization of the components in microgrid

5.2 Simulation Process

5.2.1 Main Simulation Process

Figure 5.3 shows the simulation process in Unity. When the user enters the simulation environment, a welcome window pops up and the “BACK” and “NEXT” buttons appear below the window. When the user clicks the back button, it will jump to the main interface, and when the user clicks the next button, it will enter the main environment.

Figure 5.3 Welcome window

When the user enters the main environment, user can control the perspective of the system through the up, down, left and right keys of the keyboard which makes the user operation more convenient.

In the upper left corner of Figure 5.4, a text and a button have been added. The text is used to display the time. The energy curve of the solar panel during the day is displayed by clicking the button.

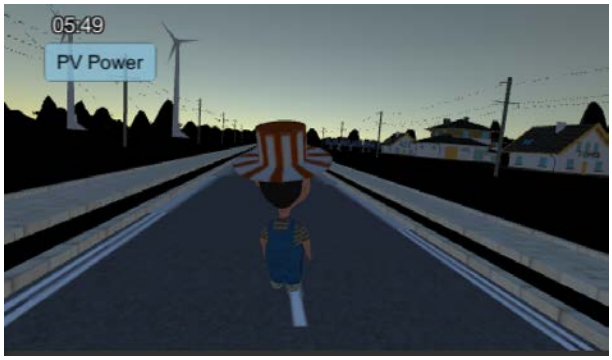

Figure 5.4 Main interface

When the user clicks the PV Power button in the upper left corner, it will jump to another sense, meanwhile add a back button in the lower right corner of the interface and click the button to return to the main interface at any time.

The global formula for estimating PV system output power is [37]

$$E = A * r * H * PR \tag{5.1}$$

Where, E is energy (kWh). A is total solar panel area (m^2). r is solar panel yield or efficiency (%). H is annual average solar radiation on tilted panel. PR is performance ratio, coefficient for losses (0.5-0.9)

5.2.2 Wind Turbine Simulation Process

Once the user moves to the location of the wind turbine, by activating the “trigger”, it will bounce off the window of the introduction of the wind turbine, the introduction information is shown on this paper chapter 4.3. The user can click the next button to continue study. At the same time, the user can back to the previous page at any time, which makes the user more convenient.

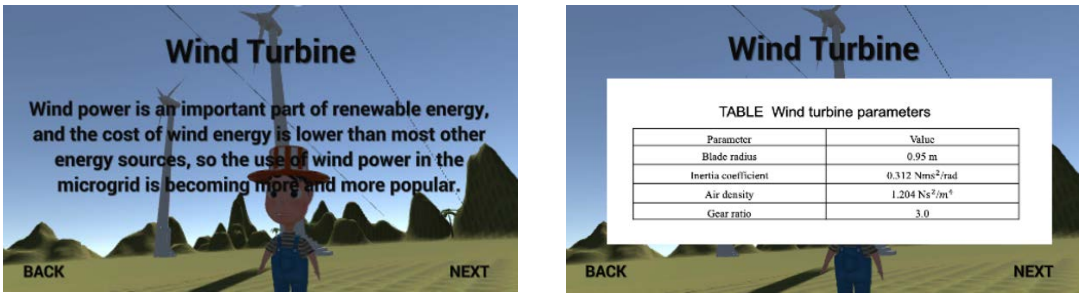

Figure 5.5 A part of wind turbine introduction window

In order to consolidate the knowledge that user have learned in the virtual environment; the quiz section is added. The user has to pass the quiz to continue study next section in the virtual environment. The user can also return to the previous lectures by clicking the back button to review the knowledge again. Moreover, the user can also click the check answer button to view the correct answer after finished the quiz. The sample quiz question is shown in Figure5 .7.

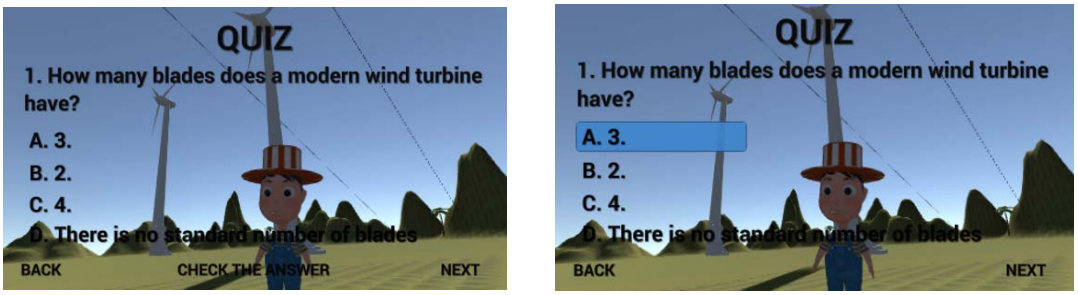

Figure 5.6 The sample quiz section

5.2.3 Solar Panel Simulation Process

The solar panel change their angle as the sun changes throughout the day to make sure maximum absorption of solar energy. The energy absorbed by solar energy changes as shown above.

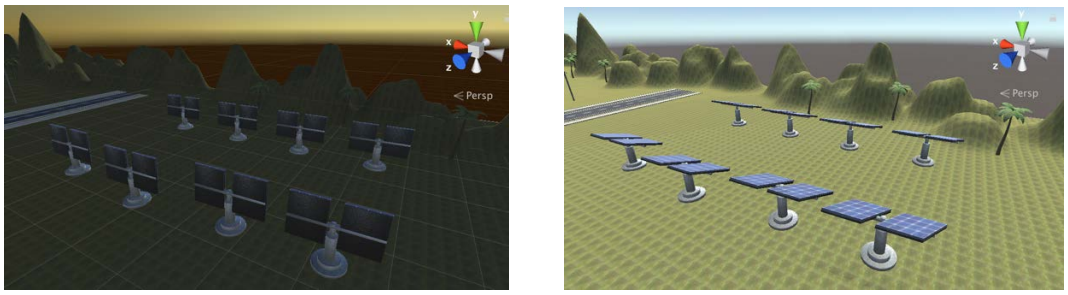

Figure 5.7 Solar panel simulation

Similar to wind turbine, when the user approaches the solar panel to trigger a collision, the introduction interface of the solar panel will pop up. When the user sees the full introduction, it will pop out of the quiz section window (Figure 5.9)

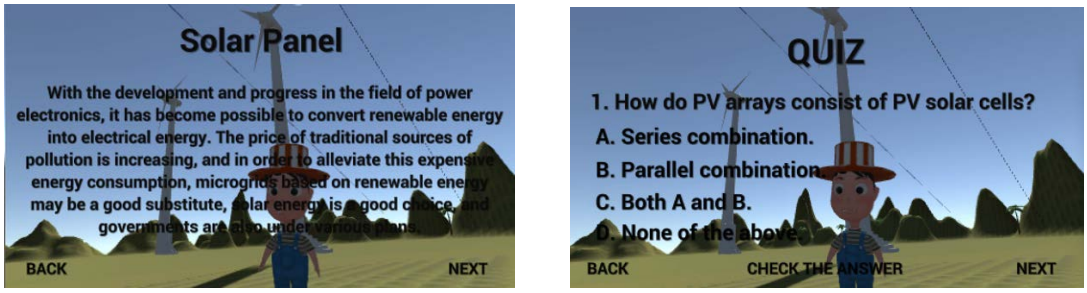

Figure 5.8 Solar panel quiz section

5.3 Conclusion and Future Work

This thesis paper introduces the traditional droop control of the island microgrid. Firstly, the basic principle of droop control is introduced. The power transmission and voltage and current double loop control of the strategy are designed. Finally, it is concluded that the traditional droop control is biased due to the difference in impedance of the transmission line and the droop coefficient, and the voltage frequency and amplitude will be deviated. It is difficult to achieve reasonable distribution of the reactive power and active power of the load. Therefore, it is necessary to further improve the traditional droop control. In the future, more advanced control methods will be adopted. Meanwhile, in the future, the droop control will be added in Unity3D. And the main purpose of Unity3d system can be used as the demonstration to attract more students in power engineering and training power engineer.

REFERENCES

[1] L. Roine, K. Therani, Y. Sahraei Manjili, and M. Jamshidi, “Microgrid energy management system using fuzzy logic control,” *World Autom. Congr. Proc.*, pp. 462–467, 2014.

[2] B. N. Alajmi, K. H. Ahmed, S. J. Finney, and B. W. Williams, “Fuzzy-Logic-Control Approach of a Modified Hill-Climbing Method for Maximum Power Point in Microgrid Standalone Photovoltaic System,” vol. 26, no. 4, pp. 1022–1030, 2011.

[3] “World Energy Use.” [Online]. Available: https://courses.lumenlearning.com/boundless-physics/chapter/case-study-world-energy-use/.

[4] O. Power, “Fuel Saving in Coal-fired Power Plant with Augmentation of Solar Energy,” 2014.

[5] D. Khani and A. S. Yazdankhah, “Control of Inverter-interfaced Distributed Generation Systems in Different Operation Modes,” no. 4, pp. 681–684, 2010.

[6] V. S. Bhadoria, N. S. Pal, and V. Shrivastava, “A Review on Distributed Generation Definitions and DG Impacts on Distribution System,” no. November, 2013.

[7] N. Hatziargyriou, H. Asano, R. Iravani, and C. Marnay, “Microgrids,” no. July 2007.

[8] B.Lasseter, “Microgrids[distributed power generation],” in *IEEE Power Engineer*, 2001, pp. 146–149.

[9] R. Lasseter, “Microgrids,” in *IEEE Power Engineer*, 2002, pp. 305–308.

[10] I. T. Force *et al.*, “Trends in Microgrid Control,” vol. 5, no. 4, pp. 1905–1919, 2014.

[11] “Microgrid.” [Online]. Available: https://www.blueskypower.com/microgrids-2/.

[12] H. Kim, “Analysis on Output LC Filters for PWM Inverters,” vol. 3.

[13] R. W. Erickson, “Optimal Single Resistor Damping of Input Filters,” no. 1.

[14] T. Zhong, Qing-chang ; Hornik, *IN RENEWABLE ENERGY AND SMART GRID INTEGRATION IN RENEWABLE ENERGY*. 2013.

[15] Y. Sun, X. Hou, J. Yang, H. Han, M. Su, and J. M. Guerrero, “New Perspectives on Droop Control in AC Microgrid,” vol. 64, no. 7, pp. 5741–5745, 2017.

[16] Q. Zhong, S. Member, and D. Boroyevich, “Structural Resemblance Between Droop Controllers and Phase-Locked Loops,” *IEEE Access*, vol. 4, pp. 5733–5741, 2016.

[17] Q. Zhong, Y. Wang, S. Member, and B. Ren, “UDE-Based Robust Droop Control of Inverters in Parallel Operation,” vol. 64, no. 9, pp. 7552–7562, 2017.

[18] A. Engler and N. Soultanis, “control in LV-Grids.”

[19] J. Yong-kang and T. Daquan, “Design of an UAV Simulation Training and Assessment System Based On Unity3D,” 2017.

[20] R. Tredinnick, B. Boettcher, S. Smith, and S. Solovy, “Uni-CAVE : A Unity3D Plugin for Non-head Mounted VR Display Systems,” *2017 IEEE Virtual Real.*, pp. 393–394.

[21] V. Do, H. Z. Jhrphwulf, and W. Vlpxodwlrq, “Using Unity3D to Simulate VHF Sailor 3520,” pp. 3–7, 2017.

[22] Unity, “Multiplayer Networking.” .

[23] W. Microgrid, A. Nied, M. Santos, M. Cavalca, and J. Patric, “Dynamic Analysis of Small Wind Turbines Frequency Support Capability in a Low-Power,” *IEEE Trans. Ind. Appl.*, vol. 54, no. 1, pp. 102–111, 2018.

[24] K. J. Bunker, S. Member, W. W. Weaver, and S. Member, “Microgrid Frequency Regulation Using Wind Turbine Controls,” *2014 Power Energy Conf. Illinois*, pp. 1–6.

[25] K. M. G. Y. Sewwandi *et al.*, “Wind Turbine Emulator for a Microgrid,” no. 3, pp. 8–13, 2017.

[26] R. Craven, “Microgrid-tied solar power generation using three-phase IGBT inverter,” *IEEE SOUTHEASTCON 2014*, pp. 1–4, 2014.

[27] B. Singh, B. K. Panigrahi, S. Member, and G. Pathak, “Control of Wind-Solar Microgrid for Rural Electrification,” *2016 IEEE 7th Power India Int. Conf.*, pp. 1–5.

[28] B. Moran and S. Electrical, “Microgrid Load Management and Control Strategies,” *2016 IEEE/PES Transm. Distrib. Conf. Expo.*, pp. 1–4, 2016.

[29] G. Jaya and H. Habeebullah, “POWER BALANCED LOAD SHEDDING OF MICROGRID SYSTEMS USING NON- LINEAR SYSTEM STABILIZER” *2014 Int. Conf. Adv. Eng. Technol.*, pp. 1–6.

[30] Ž. Matej, D. Topi, D. Šljivac, Z. Klai, and A. Brandis, “Influence of L oad P eak S having on B attery S ystem C apacity in an I slanded B uilding M icrogrid,” *2018 Int. Conf. Smart Syst. Technol.*, pp. 247–251, 2018.

[31] G. A. Taylor, “Simulation of Power System Substation Communications Architecture Based on IEC 61850 Standard.”

[32] X. Xu, F. Dong, L. Huang, and B. P. Lam, “Modeling and Simulation of Substation-Related Outages in Power Flow Analysis,” pp. 1–5, 2010.

[33] S. X. Chen, S. Member, H. B. Gooi, S. Member, M. Q. Wang, and S. Member, “Sizing of Energy Storage for Microgrids,” vol. 3, no. 1, pp. 142–151, 2012.

[34] S. Bahramirad, W. Reder, and A. Khodaei, “Reliability-Constrained Optimal Sizing of Energy Storage System in a Microgrid,” pp. 1–7.

[35] C. Chen, S. Duan, T. Cai, B. Liu, and G. Hu, “Optimal Allocation and Economic Analysis of Energy Storage System in Microgrids,” vol. 26, no. 10, pp. 2762–2773, 2011.

[36] H. Zhou *et al.*, “and Ultracapacitor With Dynamic Energy Management in Microgrid Applications,” vol. 26, no. 3, pp. 923–930, 2011.

[37] “How to calculate the annual solar energy output of a photovoltaic system?” [Online]. Available: https://photovoltaic-software.com/principle-ressources/how-calculate-solar-energy-power-pv-systems